All-fiber Spectral Filters Based on LP_{01} - LP_{11} Mode Coupling and Applications in Wavelength Division Multiplexing and Dispersion Compensation

by

Jagannathan, Jyothikumar

Thesis submitted to the faculty of the

Virginia Polytechnic Institute and State University

in partial fulfillment of the requirements for the degree of

MASTER OF SCIENCE

in

Electrical Engineering

APPROVED:

_____

Dr. A. Safaai-Jazi, Chairman

_____ _____

Dr. T. C. Poon Dr. W. A. Scales

June, 1996

Blacksburg, Virginia

All-fiber Spectral Filters Based on LP_{01} - LP_{11} Mode Coupling and Applications in Wavelength Division Multiplexing and Dispersion Compensation

by

Jyothikumar Jagannathan

Committee Chairman: A. Safaai-Jazi

Electrical Engineering

(ABSTRACT)

All-fiber spectral filters have the advantages of providing low coupling loss and being readily integrated into fiber-optic networks. Spectral filters made of single-mode identical or dissimilar core parallel fibers provide 3-dB spectral widths on the order of 1 to 10 nm. A spectral filter made of single-mode and dual-mode fibers and operating based on coupling of power between LP_{01} and LP_{11} modes is proposed for applications as narrowband demultiplexers and as broadband mode converters with spectral widths of fraction of 1 nm to few 10 nm, respectively.

With appropriate choice of parameters, filters can be designed such that the LP_{01} mode of the single-mode fiber is phase matched with the LP_{11} mode of the dual-mode fiber at a desired wavelength. Thus, significant exchange of power between these two modes can occur. The coupled-mode theory of parallel dielectric waveguides is used to analyze the proposed filter.

Transmission expressions are derived from the governing coupled-mode equations and evaluated numerically for example cases.

Two cases corresponding to maximum power coupling at 1.33 μm and 1.55 μm wavelengths are examined. Design data and transmission characteristics versus wavelength for these two cases are presented. The influence of the distance between fiber cores on peak transmission wavelength, spectral width, and coupling length is investigated. The application of the proposed filter as mode converter, which is required in the implementation of dispersion compensation using LP_{11} mode, is elucidated.

Acknowledgments

I acknowledge the continuous encouragement, and guidance provided by my advisor Dr. Ahmad Safaai-Jazi without whom this work would not have been possible. I am deeply indebted to him.

In addition, I would also like to thank all my fellow office-mates and friends at the Materials Response Group of ESM department for their support all these years.

Table of Contents

List of Figures

List of Tables

Chapter 1

Introduction

Research on communication systems is driven by factors that strive to improve fidelity and increase the *data transmission rate - distance* product between transmitter and receiver [1]. The invention of LASER in 1962, spawned interest in making use of the enormous bandwidth available at optical frequencies, particularly in the wavelength range of 0.8 μm to 1.6 μm which corresponds to the low attenuation region of silica glass fibers. In this wavelength range, optical fibers as waveguides provide a reliable and low cost communication channel. Compared to the conventional copper wires, optical fibers have numerous advantages including low transmission loss, wide bandwidth, small size and weight, immunity from electromagnetic interference, electrical isolation, signal security, and an abundant source of raw material in silica - a compound of sand.

The light sources used in present day fiber-optic communication systems are laser diodes (LDs) and light emitting diodes (LEDs) with spectral widths of few nanometers and few tens of nanometers, respectively. Therefore, a single source fiber-optic transmission system utilizes only a small fraction of the available bandwidth of about 800 nm between 0.8 μm and 1.6 μm. Several

LED signals and tens and even hundreds of LD signals can be accommodated in this wavelength range. Simultaneous transmission of two or more optical channels over the same fiber is referred to as wavelength division multiplexing (WDM). Using WDM schemes, the information carrying capacity of a fiber-optic system can be increased drastically.

Wavelength division multiplexing has attracted considerable attention in recent years. This technique can be implemented to not only design ultra high capacity fiber-optic communication systems, but also upgrade the existing systems. A wide variety of signals like audio, video, and data (analog/digital) can be transmitted through the same single fiber in future applications by expanding the system without changing or modifying the existing optical fiber cables. WDM has also found applications in non-communication areas, such as fiber-optic sensors. Sensor multiplexing, particularly in situations such as in aircraft and spacecraft where size and weight are of great concern to engineers, is fast becoming a subject of investigation and technology development.

A WDM system requires a device to combine the optical channels at the transmitting end and another to separate different channels from each other at the receiving end. The WDM device at the transmitting side is essentially a power combiner and is referred to as a multiplexer. The device at the receiver side is called a demultiplexer and should ideally separate out various channels with negligible insertion loss and signal distortion. Both multiplexer and demultiplexer are referred to as WDM device in the literature.

Demultiplexers are usually more difficult to implement than multiplexers and thus require a more thorough design. Multiplexers in most applications are wideband directional couplers, while demultiplexers are essentially spectral filters that separate out different optical channels. They can be designed and implemented utilizing a variety of devices including wavelength selective waveguide couplers, diffraction gratings, Fabry-Perot interferometers, Mach Zehnder interferometers, and acoustooptical filters. A brief survey of the techniques and devices used in the implementation of WDM systems is provided in Chapter 2.

All-fiber spectral filters have inherently lower coupling loss and hence are advantageous. They are constructed using identical or dissimilar core fiber couplers. These fiber based couplers operate based on the principle of coupling of dominant modes of interacting fiber lightguides. The dimensions of two adjacent fibers forming the coupler can be chosen such that the dispersion curves for the dominant modes of the two fibers intersect at a desired wavelength. At this wavelength, the two modes are phase matched and exchange maximum power, while at other wavelengths the two modes do not propagate at the same velocity and thus the transfer of power is not substantial. The coupled mode theory as the foundation for coupling of power between two parallel waveguides is reviewed in Chapter 3.

Most fiber based spectral filters investigated in the past consist of two single-mode fibers. In this thesis, a directional coupler made of two unidentical fibers, one single-mode supporting the LP_{01} mode and the other a dual-mode, is proposed and investigated for filtering and mode conversion applications. As a wavelength filter, the LP_{01} - LP_{11} mode coupler offers much narrower spectral width than a coupler whose constituent fibers are single-mode. The proposed coupler may also

be used as a mode converter for dispersion compensation application. Using the coupled-mode theory of parallel waveguides, a set of differential equations governing the coupling of LP_{01} and LP_{11} modes in the proposed coupler is derived in Chapter 4. The associated coupling coefficients are calculated and the transmission function of the filter is obtained.

Various dispersion phenomena in optical fibers and the application of the proposed coupler as a mode converter for compensation of chromatic dispersion are discussed in Chapter 5. Numerical results for transmission characteristics of the coupler and for the dispersion of the LP_{11} mode are presented in Chapter 6. Design of narrowband and wideband couplers and important design considerations such as spectral width, wavelength of peak transmission, side-lobe level, and coupling length are addressed. The conclusions of this work and suggestions for further research are summarized in Chapter 7.

Chapter 2

WDM Systems and Spectral Filters

2.1 Wavelength Division Multiplexing

Wavelength Division Multiplexing (WDM) is a technique for simultaneous transmission of two or more optical signals on the same fiber. The signals from different sources are combined by a multiplexer and fed into an optical fiber which is the transmission medium. At the receiving end, different signals are separated by a demultiplexer and detected by photodetectors. The WDM scheme increases the transmission capacity of optical communication systems considerably. The two configurations of WDM systems that are possible are the *one-way* and the *two-way* transmission systems as illustrated in Fig 2.1. While the one-way system requires only one receiver or one transmitter per channel at each end, the two-way system requires both receiver and transmitter at each end of every channel.

Optical multiplexers and demultiplexers may be classified into wavelength selective and wavelength nonselective devices [2]. The wavelength selective devices are either active or passive. The active devices are implemented using multi-wavelength light sources or multi-wavelength photodiodes. On the other hand, the passive devices include angularly dispersive

devices, dielectric thin film filters (DTF), hybrid devices involving gratings and dielectric thin films, and waveguide couplers. Figure 2.2 summarizes the classification of multiplexers and demultiplexers. The wavelength selective devices work on the same principle that the WDM system is based; i.e., selective combination and separation of optical signals with different wavelengths. While multiplexers could be either wavelength selective or wavelength nonselective devices, the demultiplexers always need to be wavelength selective devices, hence their design is more complicated.

Spectral filters are wavelength selective devices and may be based on diffraction gratings, Fabry-Perot interferometers, Mach Zehnder interferometers, acoustooptic filters, or parallel coupled waveguides. The performance of a spectral filter is assessed by three properties; spectral width, side-lobe level, and insertion loss. Tuning range is also an additional important property of tunable filters.

2.2 Spectral Filters

2.2.1 Diffraction Grating Filters

Grating devices when used as demultiplexers have approximately 3 dB insertion loss and 0.5 nm passband with 35 dB of crosstalk rejection. Fine gratings with large variations in the effective

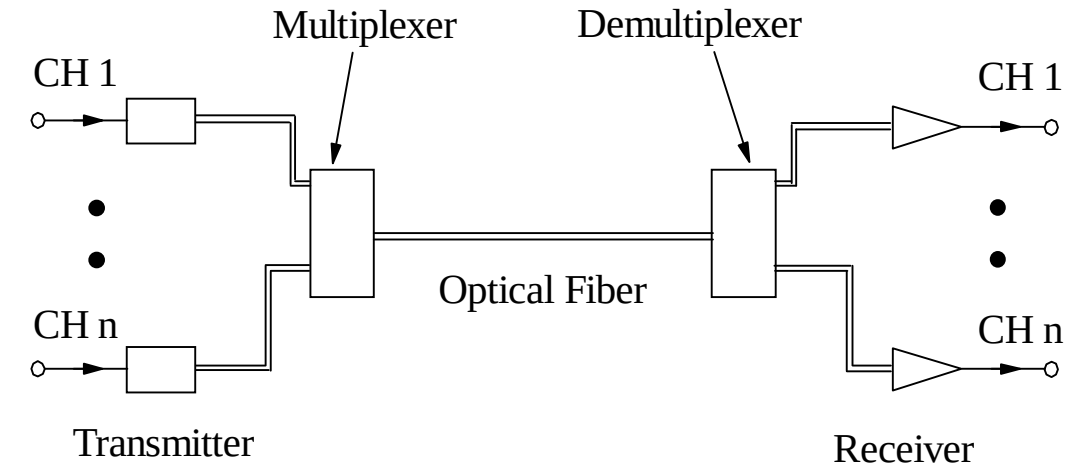

(a)

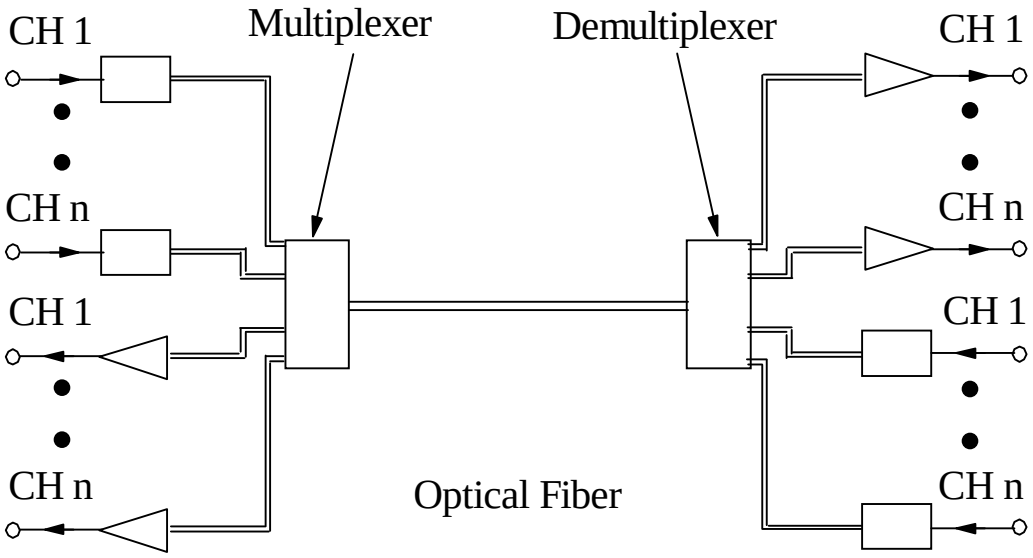

(b)

Figure 2.1 Two configurations of WDM systems; (a) one-way, and (b) two-way transmission systems.

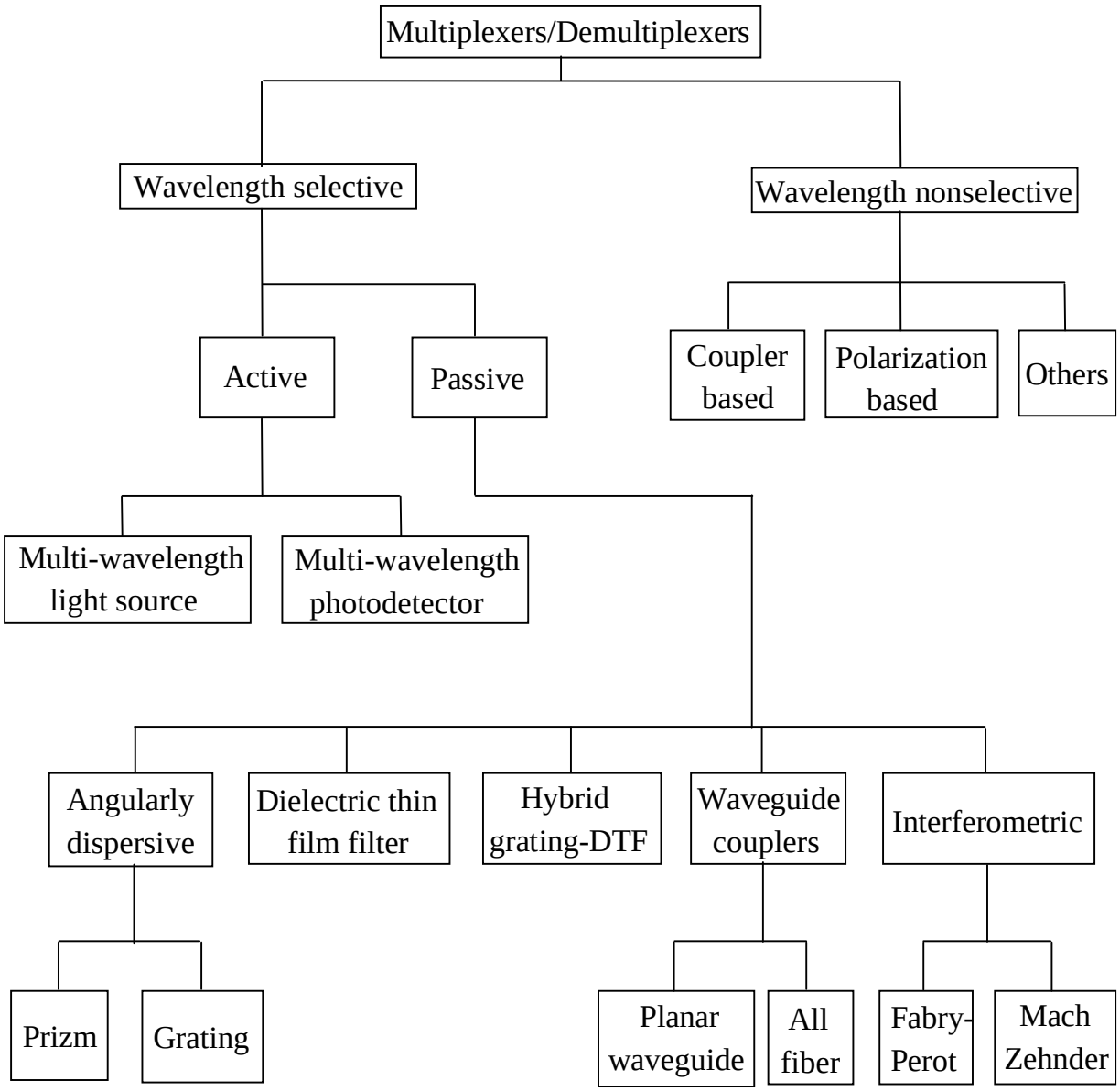

Figure. 2.2 Classification of multiplexers and demultiplexers

indices result in small filter bandwidths. For example, gratings made by periodic modulation of the refractive index next to the guide result in a bandwidth of 0.2 A and a loss of 0.5 dB for the filter [3]. All-fiber gratings written directly onto the fibers and operating at 1550 nm have been reported [4]. Gratings based on Bragg reflection are compact, tunable and have narrow passband. A spectral width of 0.4 A has been obtained at 1500 nm wavelength for a compact demultiplexer comprised of a two-waveguide directional coupler having grating reflecting regions at the two output ends [5]. The optical length of the phase shift region can be varied to tune the filter center wavelength. A narrower bandwidth of 1 nm can be achieved using two waveguides, one of which includes a quarterwave shifted distributed feedback (DFB) resonator. This filter couples only a part of the power from the other guide. In order to fully transfer the power, an additional quarterwave shifted DFB resonator is needed [6]. A tunable grating coupler/filter with 370 A tuning range has been implemented [7]. It uses two vertical stacks of INGaAsP/InP waveguides each having different effective indices and periodic grating between the guides to help in the coupling of evanescent modes. With a distributed Bragg reflector (DBR) transmission filter narrower bandwidth and increased tuning range are obtained [8]. A monolithic integrated diffraction grating demultiplexer at 1500 nm with a PIN detector array fabricated on InP substrate has been reported [9]. The gratings diffract the input beam from one guide onto an array of guides that feed the PIN array. A channel separation of less than 1 nm is achieved with only 13 dB on-chip loss.

2.2.2 Fabry-Perot Filters

Fabry-Perot (FP) filters use a resonant cavity with reflective coatings at the two ends. These filters have large spectral range, low loss and are polarization independent. An electrically tunable fiber-coupled FP interferometer can be used as a wavelength demultiplexer in single-mode systems [10]. At 1.5 μm, it provides a linewidth of 5 nm and a free spectral range (FSR) of 180 nm when the cavity separation was 6 μm. A coupled-waveguide FP resonator consisting of two parallel optical waveguides with partially reflecting mirrors at the two ends has been proposed [11]. This filter provides better mode discrimination and narrower spectral width than the conventional FP resonator. A two-section FP filter tunable around 1.5 μm has also been proposed [12]. It has the advantage that the design specifications for the tuning range are independent of the transmission bandwidth as opposed to distributed feedback (DFB) filters. This filter has a tuning range of 15 A and a bandwidth of 5 GHz. Less than -10 dB crosstalk can be achieved for a 25 channel WDM selection scheme. A standard two-fiber coupler with an intermediate multilayer FP filter proposed provides bandwidths between 20 nm and 150 nm [13]. Multistage FP etalons can be designed as discrete-time lattice filters to achieve any desired filter response [14]. They can be used in multiplexers intended for WDM and frequency division multiple access (FDMA) applications. In addition, as modulation filters, they discriminate signals based on modulation frequency as opposed to optical line frequencies.

Liquid crystal FP (LC-FP) filters have liquid crystals in their cavity. The refractive index of the cavity or the optical length is varied by applying a voltage and altering the molecular alignment of the crystals. This changes the resonant wavelength and thus the filter is tunable. A compact narrowband filter can be used as an optical tuner using LC-FP [15]. With a Peltier controller

using a low driving voltage less than 15 Volts, the filter provides a bandwidth of 0.3-1 nm, and FSR and tuning range of 50 nm. It introduces a loss of -1 dB and is designed to be low polarization dependent (< 0.3 dB).

2.2.3 Mach-Zehnder Interferometers Filters

Mach-Zehnder (MZ) interferometer filters are built using two waveguides or fibers, one serving as reference arm and another as signal arm whose refractive index is varied with the information signal. This introduces phase variations for the mode propagating in the signal arm. A sequence of seven serially arranged MZ switches using birefringence control techniques can select 1 of 128 channels [16]. Multiplexers and demultiplexers designed using the MZ devices for channel spacing between 0.008 to 250 nm can be used in dense WDM systems with 100-1000 channels [17]. A MZ interferometer using couplers as input and output channel dropping filters with weighted coupling, provides less than -30 dB side-lobe levels, and can be implemented on Si or InP [18].

2.2.4 All-Fiber Filters

All-fiber spectral filters have an inherent advantage of being easily integrated into a fiber-optic link. They also provide lower losses and lower back reflections. Several all-fiber spectral filters have been proposed and implemented based on the mode coupling phenomenon. These coupler filters include fused taper coupler [19], dissimilar core fiber coupler [20], dual-core [21], and triple-fiber couplers [22]. The fused taper coupler has a wide spectral width and can only be used to separate few well spaced channels. The dissimilar core fiber coupler on the other hand provides a narrower spectral width in which peak transmission occurs at a wavelength that

corresponds to phase matched condition between the unidentical cores. The dual-core fiber couplers can be used to design filters with different transmission wavelengths. The filter bandwidth can be narrowed by increasing the number of dual-core segments. A modified dual-core and a collinear triple-core fiber coupler filter that reduces the side-lobe level and eliminates the undesired transmission windows have also been proposed [22]. The triple-core fiber filters provide narrower bandwidth and much higher extinction ratio than the dual-core filters. The coupler proposed in [23], based on coupling of LP_{01} modes in W-index and step-index fibers, yields a spectral width of ≈ 1.5 nm at 1300 nm which is considerably narrower than that obtained from two dissimilar step-index fibers. A 3x3 collinear fiber coupler with three fibers on the same plane when used in a ring resonator, is well suited for filter applications and densely spaced WDM systems [24].

2.2.5 Other Types

Fibers made of crystalline materials such as $Y_3Al_5O_{12}$:Nd_3+ can be used to design filters that work on selective impurity absorptions [25]. These filters can be tuned by using temperature variations and it has a bandwidth of 10A at 8685A wavelength. Optical amplifiers can be used in a fiber-loop to form amplified fiber-optic recirculating delay lines (AFORDL). The active AFORDL can be used to design all-fiber filters for example, with a pole at +1 and a zero at -1 in the *z*-plane, which cannot be realized using a passive unamplified one [26]. A filter based on antiresonant reflection instead of total internal reflection in an optical waveguide called ARROW filters have been proposed [27]. The ARROW filters using SiO_2/TiO_2 have bandwidths narrower than 7 A. As compared to conventional directional coupler filter, they can have larger core size and are

much easier to fabricate due to the periodic dependence of coupling length on waveguide separation.

The interaction of optical waves and acoustic waves results in several independent pass-bands and stop-bands. The acoustooptic tunable optical filters(ATOF) can thus be implemented in dense WDM systems. A $LiNbO_3$ based polarization independent ATOF with a 1.3 nm bandwidth has been designed and demonstrated at 1500 nm [28]. A double stage ATOF filter comprising of four acoustooptic mode converters, a polarizer, and two polarization splitters provides a bandwidth of 1.4 nm with a tuning range of 76 nm around 1.55 μm [29]. A cascade of ATOF and Fabry-Perot filter provides multiple narrow passbands and a wide tuning range [30].

Chapter 3

Coupled-Mode Analysis of Parallel Optical Fibers

3.1 General Considerations

Electromagnetic waves propagating in a dielectric waveguide can be represented as a set of independent modes. The modes of two or more closely spaced dielectric waveguides can interact and exchange energy if they propagate at about the same phase velocity i.e., when their propagation constants are equal or nearly the same. The directional coupling of energy between the modes of parallel waveguides can be used to our advantage in the design of optical communication system components such as spectral filters, switches, and modulators. The mode coupling phenomenon can, in principle, be analyzed by directly employing Maxwell's equations and related boundary conditions, but it is rather lengthy and tedious. A simplified analysis based on coupled-mode theory provides approximate solutions that are sufficiently accurate for most applications of practical interest. Various phenomena in semiconductor lasers as well as in fiber and integrated optics have been described using this theory.

J.R. Pierce was the first to analyze the mode coupling phenomenon in waveguides [30]. He observed that by placing a series of obstacles in a waveguide the forward and backward propagating modes could be allowed to couple and form a wave filter. In optical waveguides for

instance, these obstacles are perturbations in the form of periodic index variations, surface irregularities, localized inhomogeneities, discontinuities, and axial nonuniformities. A general formalism of the coupled-mode theory is presented first. The formulation is then used to study the coupling of LP_{01} and LP_{11} modes between two parallel optical fibers.

3.2 General Formulation

Let us consider two sets of electromagnetic fields denoted as $\left(\vec{E}_1, \vec{H}_1\right)$ and $\left(\vec{E}_2, \vec{H}_2\right)$. Using Maxwell's equations, the Lorentz's reciprocity relation can be derived as [32]

$$\int_S \frac{\partial}{\partial z}\left(\vec{E}_1 \times \vec{H}_2^* + \vec{E}_2^* \times \vec{H}_1\right) \bullet d\vec{S} = -j\omega \int_S \left(\vec{P}_1 \bullet \vec{E}_2^*\right) dS \qquad (3.1)$$

where $\vec{P}_1$ is a polarization vector associated with field 1 and S is a z = *constant* plane. In waveguide structures, $\left(\vec{E}_2, \vec{H}_2\right)$ may be regarded as a known field associated with a given mode, while $\left(\vec{E}_1, \vec{H}_1\right)$ is an unknown field of interest in another waveguide or associated with another mode. The transverse components of field 1 may be expanded in terms of the normal modes of waveguide determined from the solution of wave equation and related boundary conditions. That is,

$$\vec{E}_{1t} = \sum_{k=1}^{N} \left[A_k(z)\, e^{-j\beta_k z} + A_{-k}(z)\, e^{j\beta_k z} \right] \vec{e}_{kt} + \int_{-\infty}^{\infty} A(\beta, z)\, e^{j\beta z}\, \vec{e}_{rt}\, d\beta \qquad (3.2a)$$

$$\vec{H}_{1t} = \sum_{k=1}^{N} \left[A_k(z)\, e^{-j\beta_k z} - A_{-k}(z)\, e^{j\beta_k z} \right] \vec{h}_{kt} + \int_{-\infty}^{\infty} A(\beta, z)\, e^{j\beta z}\, \vec{h}_{rt}\, d\beta \qquad (3.2b)$$

In (3.2a) and (3.2b), the transverse components of $\vec{E}_1$ and $\vec{H}_1$ are expressed as a superposition of N guided modes with discrete propagation constants and an integration of radiation modes with a

continuous spectrum. Since our interest is in coupling of power between guided modes only, the radiation modes can be dropped from the expansions. Now, considering the field $\left(\vec{E}_2, \vec{H}_2\right)$ to represent an *m*th forward traveling mode, substituting (3.2a) and (3.2b) in (3.1) and invoking the orthogonality properties of guided mode [33], we obtain

$$\frac{dA_m}{dz} = -j\omega \int_S \left(\vec{P}_1 \bullet \vec{E}_m^*\right) e^{j\beta_m z}\, dS \qquad (3.3)$$

Equation (3.3) can be used to study mode interactions among parallel dielectric waveguides. In such cases, the vector $\vec{P}_1$ represents perturbations which provide the mechanism for mode coupling. For example, the polarization vector resulting from perturbations of dielectric constant by the amount $\Delta\varepsilon$ is $\vec{P}(\vec{r}) = \Delta\varepsilon(\vec{r})\ \vec{E}(\vec{r})$. In most applications of practical interest, there are only two guided modes that have sufficiently close propagation constants to allow substantial exchange of power. In such cases, (3.3) is applied only to the two modes of interest and all other modes are ignored. In the next section, coupled-mode equations for two parallel waveguides are derived.

3.3 Coupled Parallel Dielectric Waveguides

The presence of a waveguide near another can be considered as a perturbation of one guide by the other and vice versa. If the two waveguides are sufficiently close to each other, there can be a transfer of power between the various modes of the two waveguides. In general, significant exchange of power is possible only between modes with nearly equal propagation constants. Let us assume that each waveguide in isolation supports only one mode. These modes are represented by fields $\left(\vec{E}_1, \vec{H}_1\right)$ for waveguide 1 and fields $\left(\vec{E}_2, \vec{H}_2\right)$ for waveguide 2. The

combination of the two waveguides may be viewed as a composite waveguide. The fields $(\vec{E}, \vec{H})$ of this composite waveguide may be approximated by the weighted sum of the unperturbed fields, i.e., the fields of individual waveguides in isolation. The reason for this approximation is that in dielectric waveguides fields decay in an exponential manner away from the core-cladding boundaries, thus in the composite waveguide the fields of weakly coupled individual guides are approximately orthogonal. The electric field of the composite waveguide is thus expressed as

$$\begin{aligned}\vec{E}(\vec{r}) &= A_1(z)\,\vec{E}_1(\vec{r}) + A_2(z)\,\vec{E}_2(\vec{r}) \\ &= A_1(z)\,\vec{e}_1(x,y)\,e^{-j\beta_1 z} + A_2(z)\,\vec{e}_2(x,y)\,e^{-j\beta_2 z}\end{aligned} \qquad (3.4)$$

A similar expression for the magnetic field $\vec{H}(\vec{r})$ can be written. The perturbation polarization vector in the composite waveguide is calculated as

$$\vec{P} = \varepsilon_0 \left[A_1(z)\,\vec{e}_1(x,y)\,e^{-j\beta_1 z}\left(n_c^2 - n_1^2\right) + A_2(z)\,\vec{e}_2(x,y)\,e^{-j\beta_2 z}\left(n_c^2 - n_2^2\right) \right] \qquad (3.5)$$

where $n_1 = n_1(\vec{r})$ and $n_2 = n_2(\vec{r})$ are the refractive index profiles of waveguides 1 and 2 in isolation, while $n_c = n_c(\vec{r})$ is the index profile of the composite waveguide.

Substituting (3.5) for $\vec{P}_1$ in (3.3) and considering $\vec{E}_m$ to be once $\vec{E}_1$ and then $\vec{E}_2$, yields

$$\frac{dA_1(z)}{dz} + j\kappa_{11} A_1(z) = -j\kappa_{12} e^{j\delta\beta z} A_2(z) \qquad (3.6)$$

$$\frac{dA_2(z)}{dz} + j\kappa_{22} A_2(z) = -j\kappa_{21} e^{-j\delta\beta z} A_1(z) \qquad (3.7)$$

where $\delta\beta = \beta_1 - \beta_2$ and

$$\kappa_{ij} = \frac{\omega \varepsilon_0}{4} \int_S \left(n_c^2 - n_j^2 \right) \vec{e}_i \bullet \vec{e}_j^{\,*} \, dS \qquad i, j = 1, 2 \qquad (3.8)$$

The coefficients κ_{ij} are the coupling coefficients. When $i = j$, the coefficients κ_{11} and κ_{22} are referred to as self coupling coefficients, while when $i \neq j$ the coefficients κ_{12} and κ_{21} are referred to as cross coupling coefficients. The coefficients κ_{11} and κ_{22} are generally much smaller than κ_{12} and κ_{21} and are usually neglected. Then, (3.6) and (3.7) reduce to

$$\frac{dA_1(z)}{dz} = -j \kappa_{12} e^{j \delta\beta z} \, A_2(z) \qquad (3.9)$$

$$\frac{dA_2(z)}{dz} = -j \kappa_{21} e^{-j \delta\beta z} \, A_1(z) \qquad (3.10)$$

Equations (3.9) and (3.10) are coupled differential equations which can be readily solved by eliminating A_1 or A_2. Eliminating A_2, we obtain

$$\frac{d^2 A_1(z)}{dz^2} - j \delta\beta \frac{dA_1(z)}{dz} + \kappa_{12} \, \kappa_{21} \, A_1(z) = 0 \qquad (3.11)$$

The solution of (3.11), assuming that A_1 ($z = 0$) = 0; i.e., the fields and hence the power in waveguide 1 are zero at $z = 0$, is obtained as

$$A_1(z) = A_0 \, e^{j \frac{\delta\beta}{2} z} \sin(S z) \qquad (3.12)$$

where A_0 is a constant coefficient, and

$$S = \left[\left(\frac{\delta\beta}{2} \right)^2 + \kappa_{12} \, \kappa_{21} \right]^{\frac{1}{2}}. \qquad (3.13)$$

Substituting (3.12) in (3.9), the solution for $A_2(z)$ is determined as

$$A_2(z) = \frac{A_0}{\kappa_{12}} \left[j S \cos(S z) - \left(\frac{\delta\beta}{2} \right) \sin(S z) \right]. \qquad (3.14)$$

The power flow in waveguides 1 or 2 is proportional to $|A_1(z)|^2$ or $|A_2(z)|^2$, respectively. The power expressions for the two waveguides are expressed as

$$P_1(z) = P_0 \frac{|\kappa_{12}|^2}{|S|^2} \sin^2(Sz) \tag{3.15}$$

$$P_2(z) = P_0 \left[\cos^2(Sz) + \left(\frac{\delta\beta}{2S}\right)^2 \sin^2(Sz) \right] \tag{3.16}$$

where $P_0 = 4 |A_0|^2 S^2 / |\kappa_{12}|^2$. The results presented in (3.12) - (3.16) are valid for two arbitrary parallel waveguides. They will be used in the next chapter to study mode coupling between two fibers, one supporting the LP_{01} mode and the other the LP_{11} mode.

Chapter 4

Analysis of LP_{01} - LP_{11} Mode Coupling

Let us consider two parallel fibers, referred to as fiber 1 and fiber 2, with core radii a_1 and a_2 and refractive indices n_1 and n_2, respectively. The two fibers have a common cladding of refractive index n_o and their axes are separated by a distance d. Fig 1 illustrates the geometry, parameters, and index profiles of the two fibers. Fiber 1 is dual-mode capable of supporting both LP_{01} and LP_{11} modes, while fiber 2 is single-mode and supports only the fundamental LP_{01} mode. All light power is initially in fiber 2 assuming the LP_{01} mode distribution, but is coupled into fiber 1 and, at the same time, converted into LP_{11} mode over the coupling region. Our aim is to analyze the exchange of power between LP_{01} mode of one fiber and LP_{11} mode of the other. The fields of LP_{11} mode in fiber 1 are denoted as $\vec{E}_1$ and $\vec{H}_1$, while those of LP_{01} mode in fiber 2 are denoted as $\vec{E}_2$ and $\vec{H}_2$. It is further assumed that both *LP* modes are x-polarized.

The propagation constant β_{01} of LP_{01} mode in the single-mode fiber is assumed to be substantially different from the propagation constant of LP_{01} mode in the dual-mode fiber. For

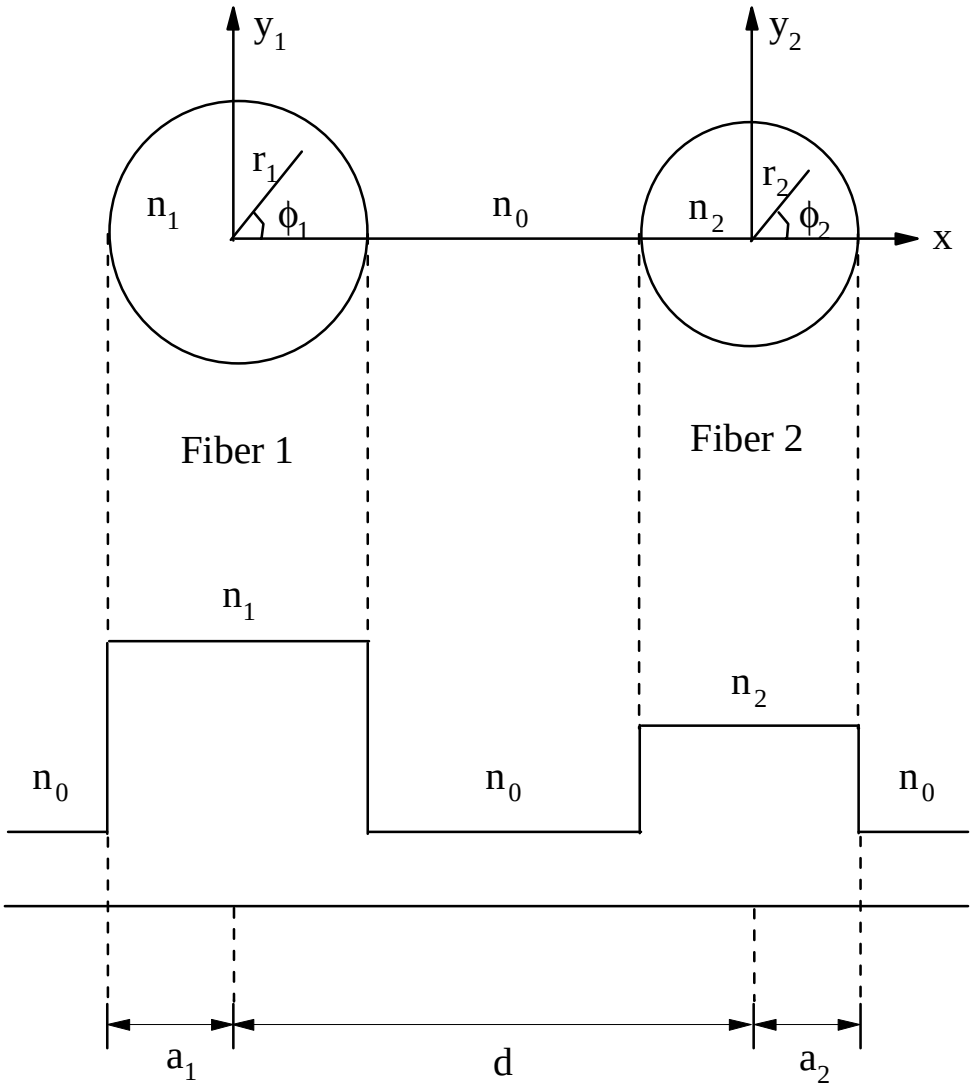

Figure 4.1. Geometry, coordinates, and index profiles for the two coupled parallel fibers.

the fiber parameters chosen, this condition is easily met; see Figs. 6.1 and 6.6. This assumption allows us to rule out any exchange of power between LP_{01} modes of the two fibers over the wavelength range of interest (1.2 μm < λ < 1.6 μm). On the other hand, β_{01} can be equal to the propagation constant β_{11} of LP_{11} mode in the dual-mode fiber at certain wavelengths; for example, at λ = 1.33 μm or 1.55 μm. This can be achieved by the appropriate choice of parameters in the design of the two fibers. Thus, the exchange of power between LP_{01} mode of the single-mode fiber and the LP_{11} mode of the dual-mode fiber is possible and is expected to be maximum at or near the wavelength where these two modes are phase matched.

4.1 Coupling Coefficients

To calculate the coupling coefficients κ_{12} and κ_{21}, the electric fields for the LP_{11} and LP_{01} modes in fibers 1 and 2 are required. Since optical fibers are weakly guiding structures with small index difference between their core and cladding, the axial field components are very small compared to the transverse components and thus neglected [34]. The transverse fields are *x* or *y* polarized. Here, *x*-polarization is considered; that is, $\vec{e}_{1t} = e_{1x}\,\hat{a}_x$ and $\vec{e}_{2t} = e_{2x}\,\hat{a}_x$. The electric field expression for the LP_{11} mode in fiber 1 is [33]

$$e_{1x} = \begin{cases} C_1 \left[J_1(u_1 r_1) / J_1(U_1) \right] \cos\phi_1, & r_1 < a_1 \\ C_1 \left[K_1(w_1 r_1) / K_1(W_1) \right] \cos\phi_1, & r_1 > a_1 \end{cases} \tag{4.1}$$

and for the LP_{01} mode in fiber 2 is

$$e_{2x} = \begin{cases} C_2 \left[J_0(u_2 r_2) \,/\, J_0(U_2) \right], & r_2 < a_2 \\ C_2 \left[K_0(w_2 r_2) \,/\, K_0(W_2) \right], & r_2 > a_2 \end{cases} \tag{4.2}$$

where J_o and J_1 are Bessel functions of the first kind, K_o and K_1 are modified Bessel functions of the second kind, C_1 and C_2 are constant coefficients, and U_1, U_2, W_1, and W_2 are defined as

$$U_1 = u_1 a_1 = k_0 a_1 \sqrt{n_1^2 - \bar{\beta}_{11}^2} \tag{4.3a}$$

$$U_2 = u_2 a_2 = k_0 a_2 \sqrt{n_2^2 - \bar{\beta}_{01}^2} \tag{4.3b}$$

$$W_1 = w_1 a_1 = k_0 a_1 \sqrt{\bar{\beta}_{11}^2 - n_0^2} \tag{4.3c}$$

$$W_2 = w_2 a_2 = k_0 a_2 \sqrt{\bar{\beta}_{01}^2 - n_0^2} \tag{4.3d}$$

In the above definitions, $k_o = 2\pi/\lambda$ is the free-space wavenumber, and $\bar{\beta}_{11} = \beta_{11}/k_0$ and $\bar{\beta}_{01} = \beta_{01}/k_0$ are the normalized propagation constants of LP_{11} and LP_{01} modes, respectively.

The constant coefficients C_1 and C_2 are determined such that the power of each mode is normalized to unity. That is

$$\frac{1}{2} \int_{S_1} e_{1x} \, h_{1y} \, dS_1 = \frac{1}{2} \int_{S_2} e_{2x} \, h_{2y} \, dS_2 = 1 \tag{4.4}$$

The expressions for C_1 and C_2 are given in the Appendix A. Now, substituting (4.1) and (4.2) in (3.8) and performing the integrations, the coupling coefficients κ_{12} and κ_{21} are obtained as

$$\kappa_{12} = \sqrt{\frac{2\left(n_2^2 - n_0^2\right)}{n_1 \, n_2}} \frac{K_1(w_1 d)}{K_1(W_2)\sqrt{K_0(W_1) K_2(W_1)}} \frac{U_1 \, U_2}{a_1 \, V_1} \frac{1}{U_2^2 + \bar{W}_1^2} \cdot \left\{ \bar{W}_1 K_0(W_2) I_1(\bar{W}_1) + W_2 K_1(W_2) I_0(\bar{W}_1) \right\} \tag{4.5}$$

$$\kappa_{21} = \sqrt{\frac{2\left(n_1^2 - n_0^2\right)}{n_1\, n_2}}\, \frac{K_1\left(w_2\, d\right)}{K_1\left(W_2\right)\sqrt{K_0\left(W_1\right) K_2\left(W_1\right)}}\, \frac{U_1\, U_2}{a_2\, V_2}\, \frac{1}{U_1^2 + \overline{W_2}^2} \cdot \left\{W_1\, K_0\left(W_1\right) I_1\left(\overline{W_2}\right) + \overline{W_2}\, K_1\left(W_1\right) I_0\left(\overline{W_2}\right)\right\} \tag{4.6}$$

where $\overline{W_1} = w_1\, a_2$, $\overline{W_2} = w_2\, a_1$, $V_1^2 = U_1^2 + W_1^2$, and $V_2^2 = U_2^2 + W_2^2$. The details for the derivation of coupling coefficients are given in the Appendix B. It can be quickly verified from (4.5) and (4.6) that the coupling coefficients κ_{12} and κ_{21} are equal when $n_1 = n_2$ and $a_1 = a_2$ as expected.

4.2 Transmission Function

The transmission characteristics $T(\lambda)$ is defined as the ratio of power output from fiber 1 at $z = L$ to power input into fiber 2 at $z = 0$.

$$T(\lambda) = \frac{\text{Power output from fiber 1}}{\text{Power input into fiber 2}} = \frac{P_1\left(z = L\right)}{P_2\left(z = 0\right)}$$

$$= \frac{\left|\kappa_{12}\right|^2}{\left|S\right|^2} \sin^2\left(S\, L\right) \tag{4.7}$$

where

$$S = \left[\left(\frac{\beta_{11} - \beta_{01}}{2}\right)^2 + \kappa_{12}\, \kappa_{21}\right]^{\frac{1}{2}}$$

and L is the coupling length. The transmission function $T(\lambda)$ is a function of wavelength through S. The coupling coefficients as calculated in (4.5) and (4.6) are substituted in (4.7). The transmission characteristics of the coupler can now be obtained for a specific wavelength range

and fiber parameters. Narrowband and broadband spectral filters can be designed by suitably selecting these parameters. It can be noted from (4.7) that maximum power is transferred from fiber 2 to fiber 1 over a length $L_c = \pi/(2S)$. The coupler can thus function as a power transferor, and as a spectral filter that selectively transfers power. Furthermore, maximum transfer of power occurs near a wavelength that corresponds to $\delta\beta = \beta_{11} - \beta_{01} = 0$. The optimum length $L = \pi/(2S)$ that is required for the optical filter is dependent on the wavelength since S is a function of wavelength. Thus, different wavelengths of the same signal require different optimum physical coupler lengths for efficient power transfer. In other words, for a particular physical length the filter passes only certain wavelengths efficiently. Initially all the power is fed into fiber 2 and ideally all of it must be transferred to fiber 1 after traveling a distance L in the coupler portion. Before proceeding further to the design and numerical simulation of various spectral filters and their characteristics, we need to examine the implications of LP_{11} mode not being a true mode.

4.3 Effect of the Pseudomode Nature of LP_{11}

Most applications of coupled-mode theory to parallel fibers have been limited to LP_{01} modes in both fibers. The LP_{01} mode is a true mode and corresponds to the vector HE_{11} mode. In the case of LP_{11} mode, and in general all LP_{lm} modes with $l \geq 1$, caution must be exercised because they are not true modes. In fact, LP_{11} mode is obtained by superimposing the vector mode pairs (TE_{01}, HE_{21}) or (TM_{01}, HE_{21}). In a weakly guiding fiber, the three vector modes TE_{01}, TM_{01}, and HE_{21} have almost the same propagation constants and are nearly degenerate. If the degeneracy were exact, there would have been no problem, but even a small difference between the propagation

constants of the modes constituting LP_{11} mode causes interference. For this reason, the mode coupling between LP_{01} mode of the single-mode fiber and LP_{11} mode of the dual-mode fiber should be considered as a three-mode coupling problem. The amplitude coefficients and the corresponding propagation constants of the three modes are denoted as

Dual-Mode Fiber:	Mode A	$a_1(z)$,	β_1
	Mode B	$\bar{a}_1(z)$,	$\bar{\beta}_1$
Single-Mode Fiber:	Mode C	$a_2(z)$,	β_2

where mode A is TE_{01}, or TM_{01}, mode B is HE_{21}, and mode C is HE_{11}.

Let us define $\delta\beta$, $\Delta\beta$, and $\Delta\bar{\beta}$ as

$$\delta\beta = \bar{\beta}_1 - \beta_1 \tag{4.8a}$$

$$\Delta\beta = \beta_1 - \beta_2 \tag{4.8b}$$

$$\Delta\bar{\beta} = \bar{\beta}_1 - \beta_2 = \delta\beta + \Delta\beta \tag{4.8c}$$

Substituting the appropriate fields of the three modes A, B, and C into the reciprocity relation (3.3) and upon further simplification, the following two sets of coupled differential equations are obtained.

$$\frac{d}{dz}\left(a_1 + \bar{a}_1\, e^{-j\delta\beta z} \right) = -j\, a_2\, \kappa_{12}\, e^{j\Delta\beta z} \tag{4.9a}$$

$$\frac{da_2}{dz} = -j\, \kappa_{12} \left(a_1 + \bar{a}_1\, e^{-j\delta\beta z} \right) e^{-j\Delta\beta z} \tag{4.9b}$$

and

$$\frac{d}{dz}\left(\bar{a}_1 + a_1\, e^{-j\delta\beta z} \right) = -j\, a_2\, \kappa_{12}\, e^{j\Delta\bar{\beta} z} \tag{4.10a}$$

$$\frac{da_2}{dz} = -\,j\,\kappa_{12}\left(\,\bar{a}_1 + a_1\,e^{\,j\,\delta\beta\,z}\,\right)e^{-j\,\overline{\Delta\beta}\,z} \qquad (4.10b)$$

It is realized that the term $a_1 + \bar{a}_1\,e^{-j\,\delta\beta\,z}$, is in fact, the amplitude term for the LP_{11} mode with phases referred to mode A, whereas the term $\bar{a}_1 + a_1\,e^{\,j\,\delta\beta\,z}$ is the amplitude with phases referred to mode B. Both sets of equations (4.9) and (4.10) have the same format as (3.9) and (3.10), and thus the power expressions $P_{11}(z)$ and $P_{01}(z)$ resulting from solution of (4.9a) and (4.9b) will be the same as $P_1(z)$ and $P_2(z)$ in (3.15) and (3.16), respectively, with $S = \left[\left(\frac{\Delta\beta}{2}\right)^2 + \kappa_{12}\,\kappa_{21}\right]^{\frac{1}{2}}$ where $\Delta\beta = \beta_1 - \beta_2$. Likewise, the solution of (4.10a) and (4.10b) for power expressions $\bar{P}_{01}(z)$ and $\bar{P}_{11}(z)$ will be obtained from (3.9) and (3.10) with S replaced with

$$\bar{S} = \left[\left(\frac{\overline{\Delta\beta}}{2}\right)^2 + \kappa_{12}\,\kappa_{21}\right]^{\frac{1}{2}} = \left[\left(\frac{\Delta\beta}{2} + \frac{\delta\beta}{2}\right)^2 + \kappa_{12}\,\kappa_{21}\right]^{\frac{1}{2}}$$

Ideally, $P_{01}(z)$ and $P_{11}(z)$ should be equal to $\bar{P}_{01}(z)$ and $\bar{P}_{11}(z)$, respectively; but in reality they are not equal because these modes are only approximately degenerate. However, if $S \cong \bar{S}$, then the two sets of results are very nearly the same.

Our interest is primarily in the spectral characteristic of $P_{11}(\lambda)$ or $\bar{P}_{11}(\lambda)$; that is, variations of transferred power from the single-mode fiber into the dual-mode fiber versus wavelength. The important features are the coupling length L_c for maximum transfer of power, the spectral width, and the wavelength corresponding to peak transmission. The coupling length (for both P_{11} and $\bar{P}_{11}$ to be maximum) is

$$L_c = \frac{\pi}{2S}\bigg|_{\Delta\beta = 0} = \frac{\pi}{2\bar{S}}\bigg|_{\Delta\bar{\beta} = 0} = \frac{\pi}{2\sqrt{\kappa_{12}\ \kappa_{21}}}$$

The spectral widths for both P_{11} and $\bar{P}_{11}$ are essentially equal, because $P_{11}(\lambda)$ and $\bar{P}_{11}(\lambda)$ have identical mathematical forms and κ_{12}, κ_{21}, and $\Delta\beta$ are nearly constant throughout and in the neighborhood of main transmission window (i.e., about the wavelength of peak transmission). The wavelength corresponding to peak transmission for $P_{11}(\lambda)$ and $\bar{P}_{11}(\lambda)$ are slightly different. These wavelengths correspond to $\Delta\beta = 0$ and $\Delta\bar{\beta} = 0$ and differ by only several nanometers. It may be concluded that $\bar{P}_{11}(\lambda) = P_{11}(\lambda - \delta\lambda)$, where $\delta\lambda$ is the error due to the true mode approximation of the LP_{11} mode in the coupled-mode analysis. Fortunately, this error is within acceptable limits. In conclusion, the coupled-mode analysis applied directly to the LP_{11} pseudomode, rather than to its constituent true modes, provides accurate results for coupling length and spectral width. The transmission wavelength is predicted accurate to several nanometers.

Chapter 5

Dispersion Compensation

Attenuation and dispersion are two limiting effects that need to be dealt with in fiber optic communication systems. The problem of attenuation can be overcome with the availability of optical amplifiers. Most of the optical fibers that are in service today were designed for low dispersion at the wavelength of 1.3 μm. However, minimum attenuation in silica glass optical fibers occurs at the wavelength of 1.55 μm. Optical fibers designed to operate at 1.3 μm result in substantial dispersion at 1.55 μm which should be compensated if the same *bit rate - distance* product is to be maintained. Currently there exists two kinds of techniques to compensate for dispersion, active and passive. The active technique involves implementation of pre-chirping and frequency-to-amplitude conversion of source signals or pulses. The passive technique, on the other hand, makes use of passive elements like specially designed optical elements, fibers and couplers to compensate for dispersion [35]. In this chapter, we look at one such passive technique of utilizing the proposed LP_{01} - LP_{11} mode coupler to compensate for chromatic dispersion. But before proceeding with the details, various dispersion phenomena in optical fibers are briefly reviewed.

5.1 Dispersion Effects

Information signals are distorted as they propagate along the fiber. Various dispersion effects contribute to these distortions, and depending on whether they occur within the same mode or between different modes, they are referred to as *intramodal* and *intermodal* dispersion [34]. Intramodal or chromatic dispersion occurs when the signals carried by a particular mode of a fiber gets dispersed due to the material and the waveguide characteristics of the fiber. If the refractive index of the fiber varies with wavelength, different spectral components of the signal carried by a mode travel at different velocities along the fiber and thus arrive at the receiving end at different times, thereby distorting the output signal. This type of dispersion which is due to the variation of the refractive index of the material with wavelength is known as *material dispersion*. The signal carried by a fiber is also distorted due to the waveguide characteristics of the fiber, the resulting dispersion effect is known as *waveguide dispersion*. On the other hand, the input signal can be carried along the fiber by more than one mode. In a multimode fiber, each mode has a different propagation constant β and hence travels along the fiber at a different velocity. The dispersion in this case is known as intermodal dispersion. For the two-fiber coupler under investigation here, we can assume that only one mode is excited in each fiber from the fact that in order for different modes to exist in a fiber they need an appropriate excitation source or mechanism. It is emphasized that power from LP_{01} mode of the single-mode fiber is essentially coupled to the LP_{11} mode of the dual-mode fiber and not to its LP_{01} mode because of phase matching conditions.

5.2 Chromatic Dispersion

The two components of chromatic dispersion are material and waveguide dispersion. To assess the material dispersion, variations of refractive indices of materials used in optical fiber structure versus wavelength are required. The wavelength dependence of refractive index is described by the Sellmeier equation expressed as [36]

$$n^2(\lambda) = 1 + \sum_{i=1}^{3} \frac{A_i \lambda^2}{\lambda^2 - \lambda_i^2} \tag{5.1}$$

where A_i and λ_i are Sellmeier coefficients and are obtained by measurements. These coefficients for 25 silica based glass materials are available.

The material dispersion in the absence of any waveguiding effect is obtained from [37]

$$D_{\text{mat}} = \frac{\lambda}{c} \frac{d^2 n}{d \lambda^2} \tag{5.2}$$

The waveguide dispersion in the absence of material dispersion; i.e., assuming that refractive indices of core and cladding do not vary with wavelength, is obtained from [37]

$$D_{\text{wg}} = \frac{1}{2 \pi c} \frac{d}{d \lambda} \left[\lambda^2 \frac{d \beta}{d \lambda} \right] \tag{5.3}$$

where c is the velocity of light in free space and β is the propagation constant of the fiber mode. An estimate of the chromatic dispersion is obtained by adding the waveguide and material dispersion calculated separately. This method is approximate and its accuracy may not be

adequate for broadband applications [38]. Chromatic dispersion can be more acurately calculated by incorporating refractive index variations into the characteristic equation.

For the two modes of interest, the characteristic equations are expressed as

$$\frac{J_1(U_1)}{U_1 J_0(U_1)} + \frac{K_1(W_1)}{W_1 K_0(W_1)} = 0 \text{, for } LP_{11} \text{ mode of fiber 1,} \tag{5.4}$$

$$\frac{J_0(U_2)}{U_2 J_1(U_2)} - \frac{K_0(W_2)}{W_2 K_1(W_2)} = 0 \text{, for } LP_{01} \text{ mode of fiber 2,} \tag{5.5}$$

where U_1, U_2, W_1, and W_2 have been defined in chapter 3. Equations (5.4) and (5.5) are functions of wavelength λ, propagation constant β, and refractive indices n of core and cladding materials. However, when each refractive index is replaced with the R.H.S of (5.1), the above characteristic equations become only a function of λ and β. Doing so, all wavelength dependencies are accounted for simultaneously. Then, chromatic dispersion is obtained from

$$D = \frac{1}{2\pi c}\left[2\lambda \frac{d\beta(\lambda)}{d\lambda} + \lambda^2 \frac{d^2\beta(\lambda)}{d\lambda^2}\right] \tag{5.6}$$

Equation (5.6) is used to determine chromatic dispersion for both the LP_{11} mode of fiber 1 and LP_{01} mode of fiber 2. Solving (5.4) for the first mode and using the resulting propagation constant β_{11} in (5.6), the chromatic dispersion D_{11} for the LP_{11} mode is obtained. Repeating this process by solving (5.5) for the first mode to find β_{01} and then substituting in (5.6), the chromatic dispersion D_{01} for the LP_{01} mode is obtained. It is emphasized that characteristic equations (5.4)

and (5.5) are solved numerically. Also numerical techniques are used to calculate $d\beta/d\lambda$ and $d^2\beta/d\lambda^2$.

5.3 Dispersion Compensation

Chromatic dispersion can assume both positive and negative values. Cascading two fibers with opposite sign chromatic dispersion results in reduction of total distortion over the combined length of the two fibers. A single-mode fiber designed for operation at λ = 1.3 μm results in positive dispersion if operated at λ = 1.55 μm. This dispersion can be canceled if the signal is let to propagate in a fiber with negative dispersion at λ = 1.55 μm. The LP_{11} mode of a step-index fiber generally provides negative dispersion and thus can be used for dispersion compensation purposes.

The signal carried by an existing single-mode fiber (initially designed for l = 1.3 μm but now operated at λ = 1.55 μm) is converted to a LP_{11} mode by the LP_{01} - LP_{11} mode coupler. The output of the coupler is spliced to a specially designed dual-mode fiber which provides a large negative dispersion for the LP_{11} mode. This negative dispersion causes the spread pulses to be compressed and reassume its original width over a length L' of the dispersion compensating fiber. The length L is obtained from

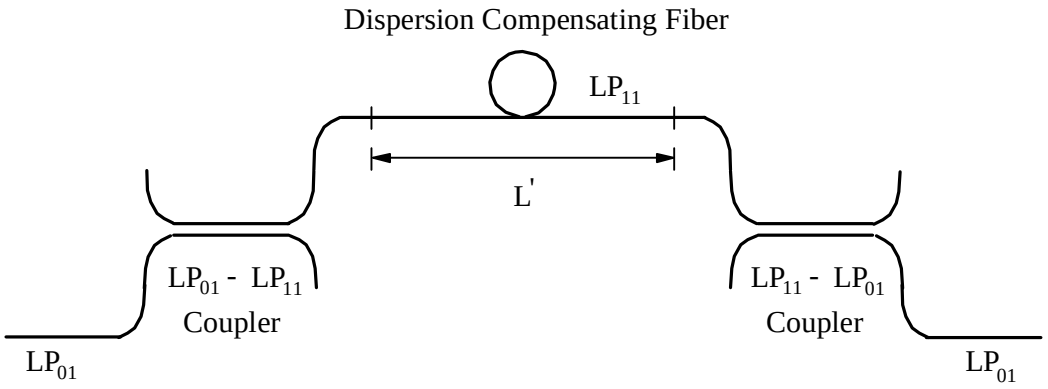

Figure 5.1 Dispersion compensation using LP_{11} mode.

$$L' = \left| \frac{D_{01}}{D_{11}} \right| L \qquad (5.7)$$

where L is the length of the 1.33 μm fiber. Another LP_{01} - LP_{11} mode coupler can convert the LP_{11} mode back to LP_{01} mode which then will be coupled into the next segment of the 1.3 μm. Fig 5.1 shows the dispersion compensation setup in a fiber-link.

Chapter 6

Numerical Results

To assess the performance of the proposed LP_{01} - LP_{11} fiber coupler for applications in wavelength filtering and dispersion compensation, numerical results based on the formulation developed in Chapter 4 are presented. Transmission characteristics for several example cases are calculated and discussed. Design of narrowband and broadband spectral filters and important design considerations such as spectral width, wavelength of peak transmission, coupling length, and side-lobe level, are addressed. The chromatic dispersion for the LP_{11} mode of several dispersion compensating fibers designed to yield large negative dispersion at 1.55 μm is also evaluated.

6.1 Transmission Characteristics

Transmission characteristics are calculated using the power transmission function $T(\lambda)$ given in (4.7) and rewritten here as

$$T(\lambda) = \frac{\left|\kappa_{12}(\lambda)\right|^2}{\left|S(\lambda)\right|^2} \sin^2\left(S(\lambda)L\right) \qquad (6.1)$$

The transmission function $T(\lambda)$, apart from being a function of wavelength, also depends on fiber parameters a_1, a_2, n_0, n_1, and n_2, fiber separation d, and coupling length L_c. Furthermore, the coupling coefficients κ_{12} and κ_{21} as well as S depend on the propagation constants of the constituent fibers. Thus, to obtain the transmission characteristics, first propagation constants β_{11} and β_{01}, for the LP_{11} and LP_{01} modes respectively, are calculated.

Two cases corresponding to peak transmission at λ = 1.33 μm and λ = 1.55 μm are considered. The parameters and material compositions of fibers, yielding a peak transmission at 1.33 μm are summarized in Table 6.1. Fig 6.1 illustrates the dispersion characteristics for $LP_{01}^{(1)}$, $LP_{11}^{(1)}$, and $LP_{01}^{(2)}$ modes, where superscripts (1) and (2) refer to fibers 1 and 2, respectively. These characteristics show variations of normalized propagation constants ($\bar{\beta} = \beta/k_0$; $k_0 = 2\pi/\lambda$) versus wavelength. It is noted that the characteristics of $LP_{01}^{(2)}$ and $LP_{11}^{(1)}$ modes intersect at λ = 1.33 μm. In other words, these two modes have the same propagation constant and thus are phase matched at λ = 1.33 μm. The dispersion characteristic for $LP_{01}^{(1)}$ mode is not needed in the calculation of transmission function, but is given here to ascertain the fact that LP_{01} mode of the two fibers have substantially different propagation constants and thus do not exchange power.

Table 6.1 Fiber parameters and material compositions for 1.33 μm filter.

Fiber	Core radius (μm)	Δ at λ = 1.33 μm	Core Material	Cladding Material
1	3.4	0.8%	13.5 m/o GeO_2 86.5 m/o SiO_2	5.8 m/o GeO_2 94.2 m/o SiO_2
2	3.1	0.4%	9.1 m/o GeO_2 90.9 m/o SiO_2	5.8 m/o GeO_2 94.2 m/o SiO_2

m/o = mole percent

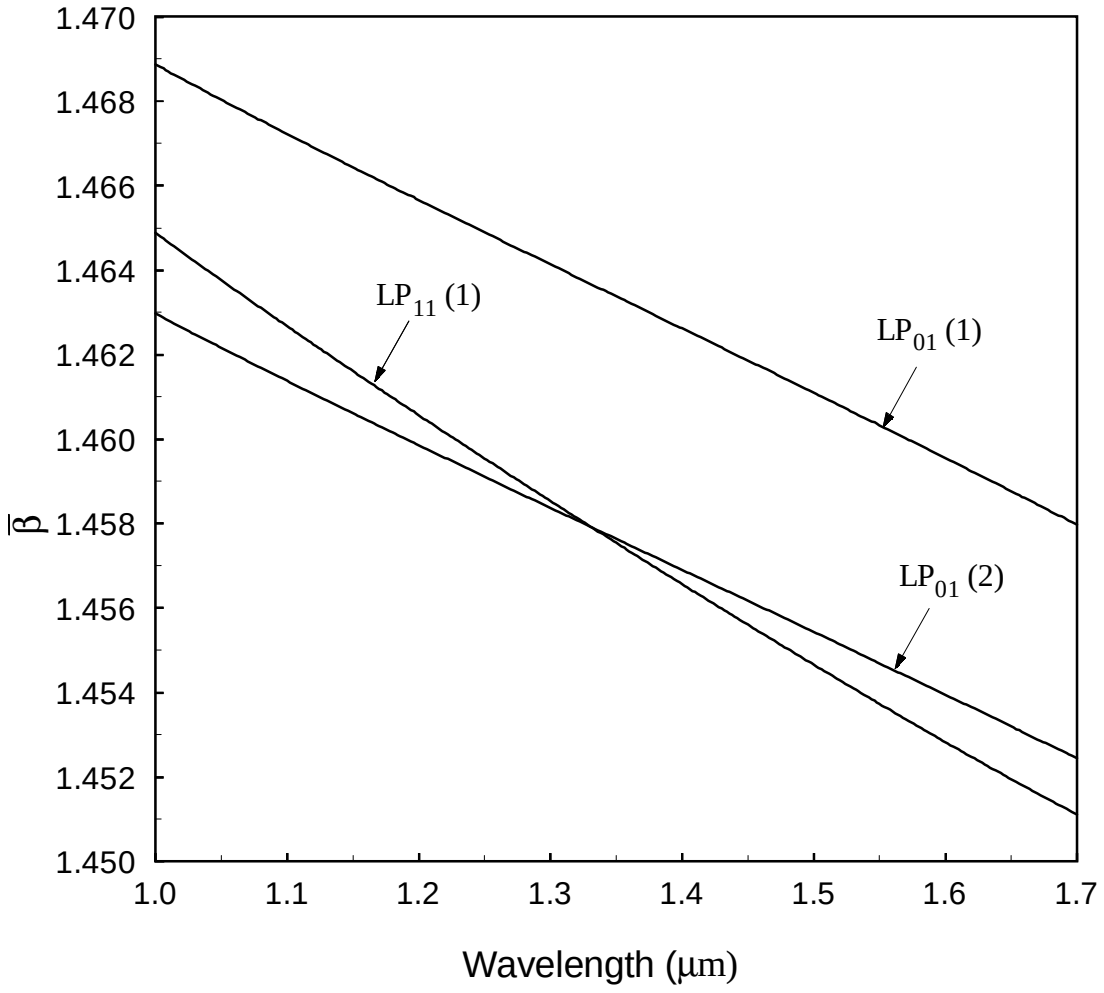

Figure 6.1 Normalized propagation constants for LP_{01} and LP_{11} modes of fiber 1 and LP_{01} mode of fiber 2. The parameters and materials of the fibers are as defined in Table 6.1.

Fig 6.2 shows the transmission characteristic $T(\lambda)$ of a 1.33 μm spectral filter with fiber parameters and materials defined in Table 6.1. As expected, peak transmission occurs at about λ = 1.33 μm. The separation of the two fiber is d = 20 μm. The half-power spectral width is $\Delta\lambda$ = 1.5 nm and the first side-lobe level is about 0.1 (-10 dB). It is noted that with these parameters, the coupler functions as a narrowband spectral filter. The spectral width of the filter $\Delta\lambda$, is primarily governed by the slope difference between the propagation constants of interacting modes as well as the fiber separation d. In fact, it is the larger slope difference between the propagation constants of LP_{01} and LP_{11} modes in the proposed coupler, compared with the slope difference for two LP_{01} modes in a coupler made of two dissimilar step-index single-mode fibers, which is responsible for narrow spectral width. Fiber separation also influences the spectral width. Reducing the separation results in an increase in the spectral width. This is clearly seen in Fig 6.3 which shows the transmission characteristic for d = 15 μm. All other parameters are the same as those in Fig 6.2. The 3-dB spectral width is about 13 nm for the wideband filter. Variations of half-power spectral width versus separation d are shown in Fig 6.4. It is noted that spectral width appears to decrease in an exponential manner with fiber separation. This behavior is attributed to the fact that for smaller separations the two fibers interact more strongly because overlapping evanescent fields are stronger, thus allowing coupling of power to take place over a wider wavelength range.

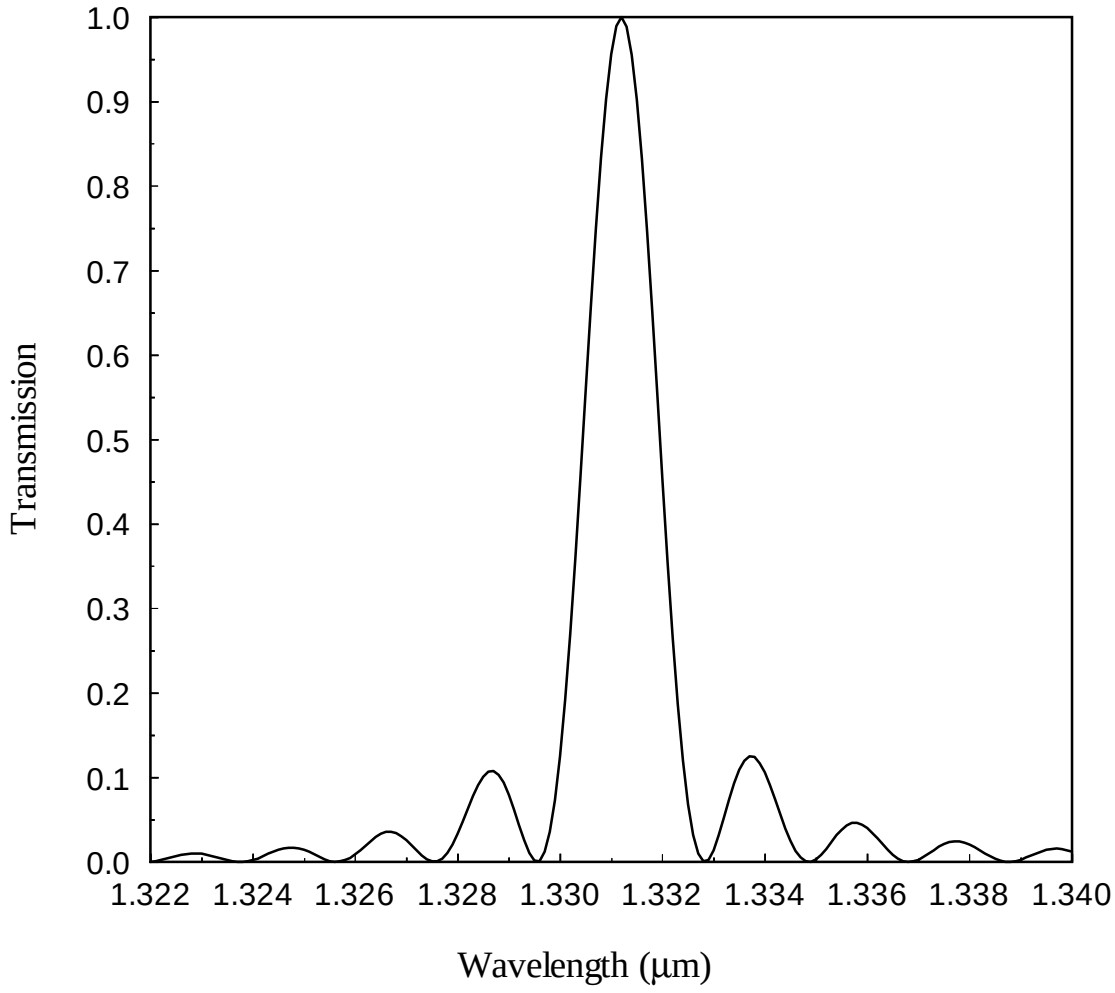

Figure 6.2 Transmission characteristic of 1.33 μm filter with fiber separation d = 20 μm. The parameters and materials of fibers are as defined in Table 6.1.

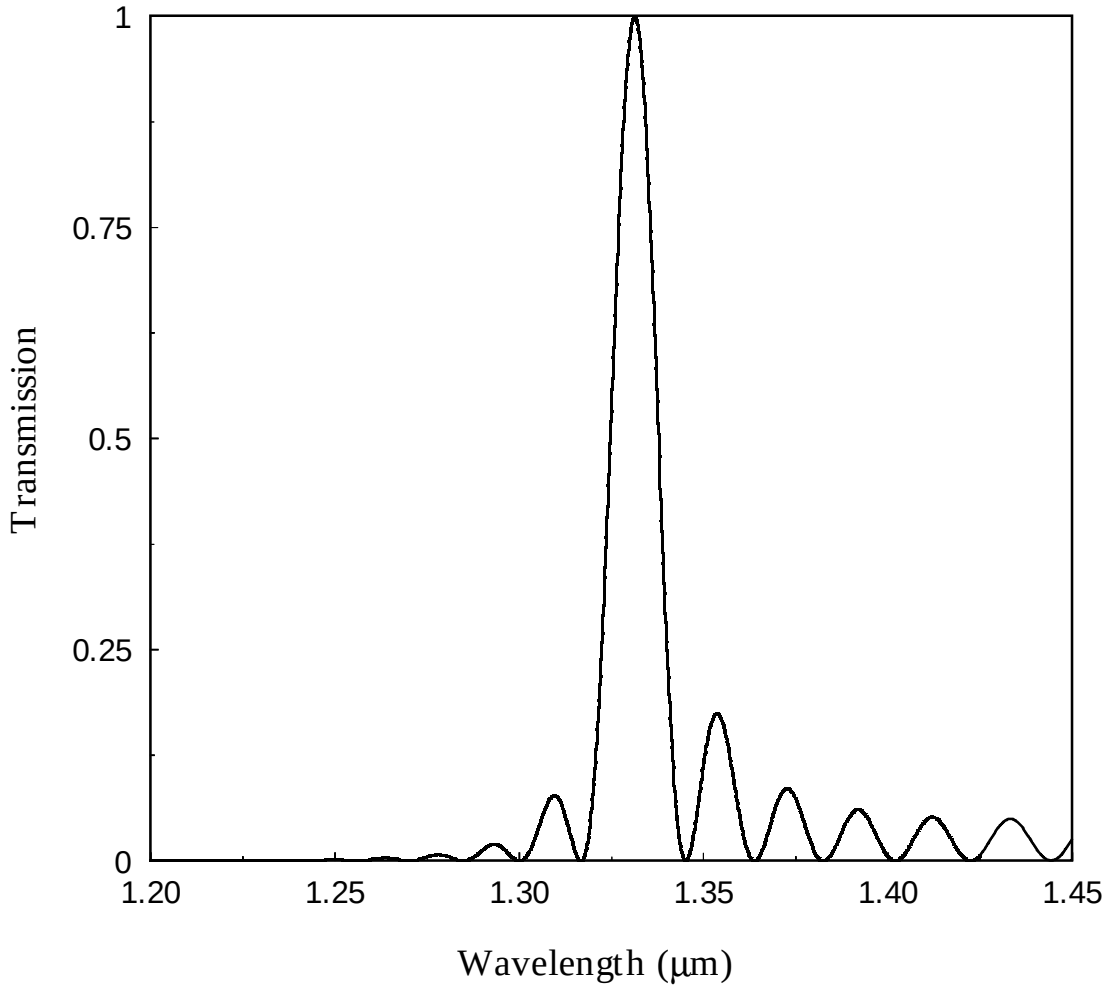

Figure 6.3 Transmission characteristic of 1.33 μm filter with fiber separation d = 15 μm. The parameters and materials of fibers are as defined in Table 6.1.

Another important design parameter is the coupling length L_c. This length is determined such that $T(\lambda)$ is maximum at the desired wavelength for peak transmission. It is clear from (6.1) that $T(\lambda_0)$ is essentially maximum when $S(\lambda_0)\, L = \pi/2$. Thus,

$$L = \pi / 2\, S\left(\lambda_0\right) \tag{6.2}$$

For this case λ_0 = 1.33 μm. The coupling length is strongly influenced by the fiber separation *d*. Fig 6.5 illustrates variations of coupling length versus separation *d*. It is apparent that *L* increases exponentially with separation *d*. Again, the reason for this behavior can be explained if it is noted that interaction of modes in the two fibers and exchange of power between them is through the evanescent fields in the common cladding region. The evanescent fields decay exponentially from the core-cladding boundaries of the fiber. Thus, the further apart the two fibers are, the weaker the interaction between them and the longer the required length for maximum transfer of power. In summary, narrower spectral widths are achieved with larger coupling lengths.

Next, spectral properties of a filter with peak transmission at λ = 1.55 μm are examined. The parameters and materials for the fibers used in this filter are summarized in Table 6.2. The dispersion characteristics of $LP_{01}^{(2)}$ and $LP_{11}^{(1)}$ modes for this case are illustrated in Fig 6.6. It Is noted that these characteristics intersect at λ = 1.55 μm and the modes are thus phase matched at this wavelength. On the other hand, the propagation constants of $LP_{01}^{(1)}$ and $LP_{11}^{(2)}$ modes are substantially different, thus practically no exchange of power between them. Transmission characteristics for fiber separations of 25 μm and 15 μm are illustrated in Figs 6.6 and 6.7, respectively. As anticipated, the peak transmission is at approximately 1.55 μm (1.541 μm to be exact). The 3-dB spectral width is about 1.1 nm for the narrowband filter and 40.8 nm for the

Table 6.2 Fiber parameters and material compositions for 1.55 μm filter.

Fiber	Core Radius (μm)	Δ at λ = 1.55 μm	Core Material	Cladding Material
1	3.85	0.8%	13.5 m/o GeO_2 86.5 m/o SiO_2	5.8 m/o GeO_2 94.2 m/o SiO_2
2	3.5	0.4%	9.1 m/o GeO_2 90.9 m/o SiO_2	5.8 m/o GeO_2 94.2 m/o SiO_2

m/o = mole percent

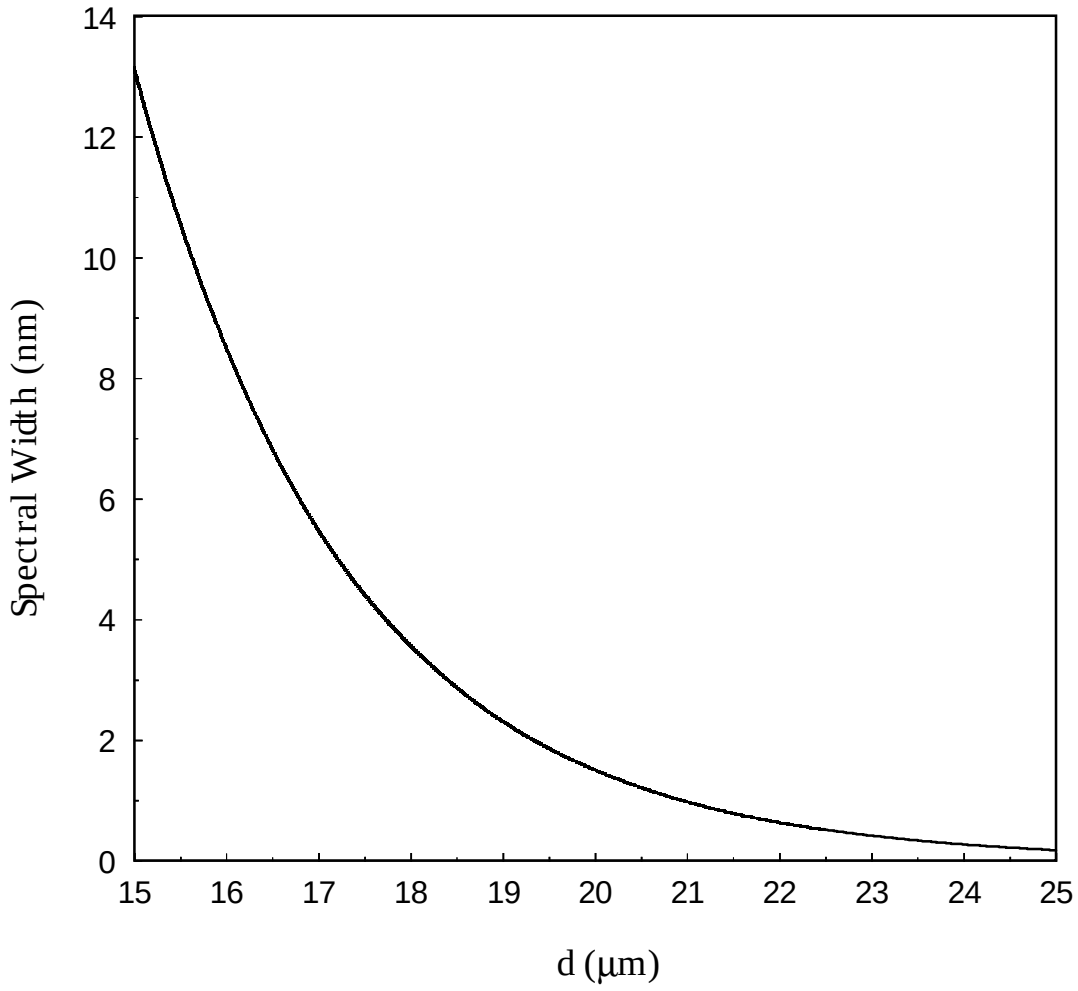

Figure 6.4 Variations of 3-dB spectral width versus fiber separation for 1.33 μm. The parameters and materials of fibers are as defined in Table 6.1.

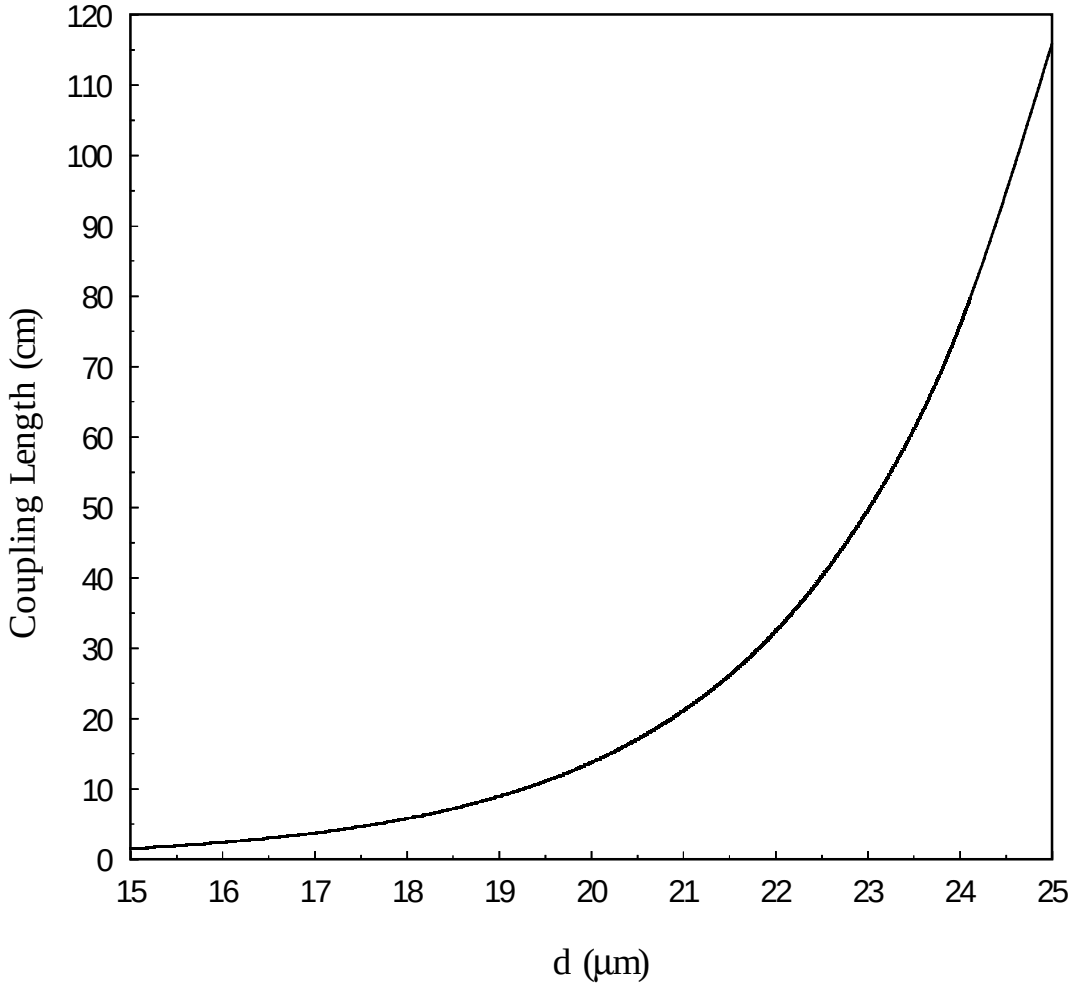

Figure 6.5 Variations of coupling length versus fiber separation for 1.33 μm. The parameters and materials of fibers are as defined in Table 6.1.

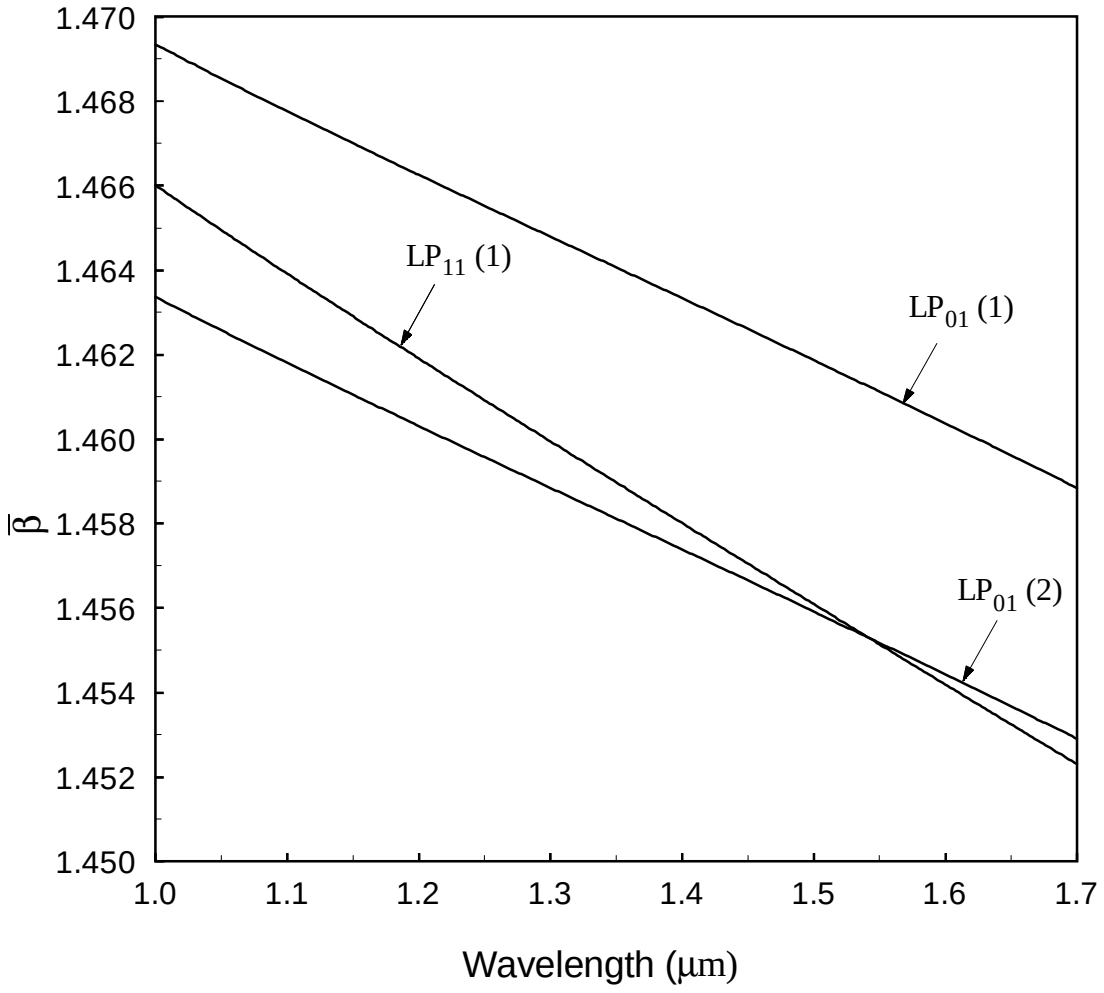

Figure 6.6 Normalized propagation constants for LP_{01} and LP_{11} modes of fiber 1 and LP_{01} mode of fiber 2. The parameters and materials of the fibers are as defined in Table 6.2.

wideband one. Variations of spectral width and coupling length for this filter are shown in Figs 6.8 and 6.9, respectively. Much of discussions on spectral width and coupling length of 1.33 μm filter are also applicable to 1.55 μm filter. However, for the same fiber separations, the spectral width of 1.55 μm filter is larger than that for the 1.33 μm filter, while the coupling length of the former filter is smaller than the latter one.

6.2 Dispersion Compensation

Let us consider a single-mode fiber designed to provide zero dispersion at 1.33 μm. When operated at λ = 1.55 μm, this fiber results in positive dispersion on the order of 13 ps/nm.km, as shown in Fig 6.11. The fiber has the same material composition as that of fiber 2 in Table 6.1, but the core radius is 3.4 μm (in order to have zero dispersion at 1.33 μm). To compensate the pulse spreading resulting from the positive dispersion at 1.55 μm, the LP_{01} mode of this input fiber is converted to the LP_{11} mode by means of coupler filter with parameters as defined in Table 6.2. The output of the coupler is connected to a dispersion compensating (DC) fiber as illustrated in Fig 5.1. The LP_{11} dispersion curves for these DC fibers are shown in Fig. 6.11. The parameters and material compositions for these fibers are summarized in Table 6.3. It is noted

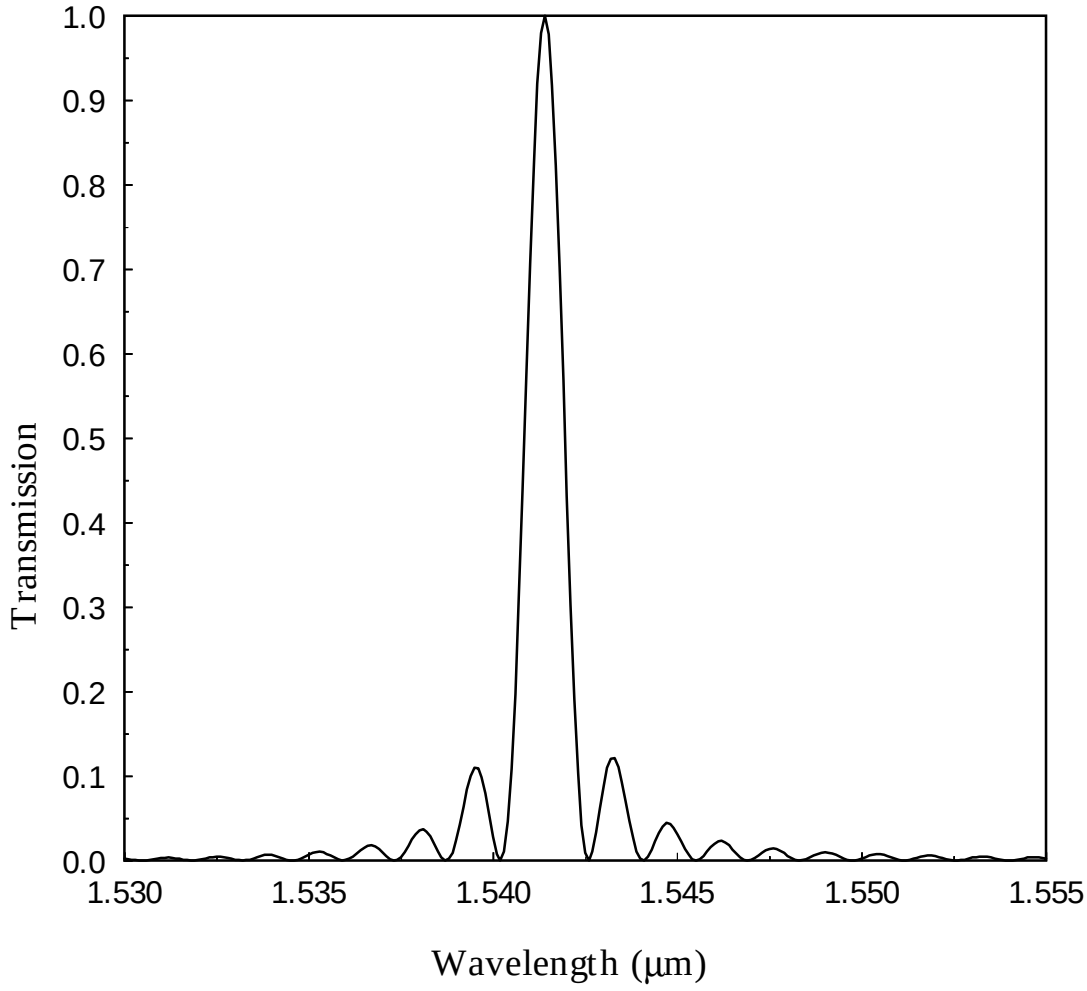

Figure 6.7 Transmission characteristic of 1.55 μm filter with fiber separation d = 25 μm. The parameters and materials of fibers are as defined in Table 6.2.

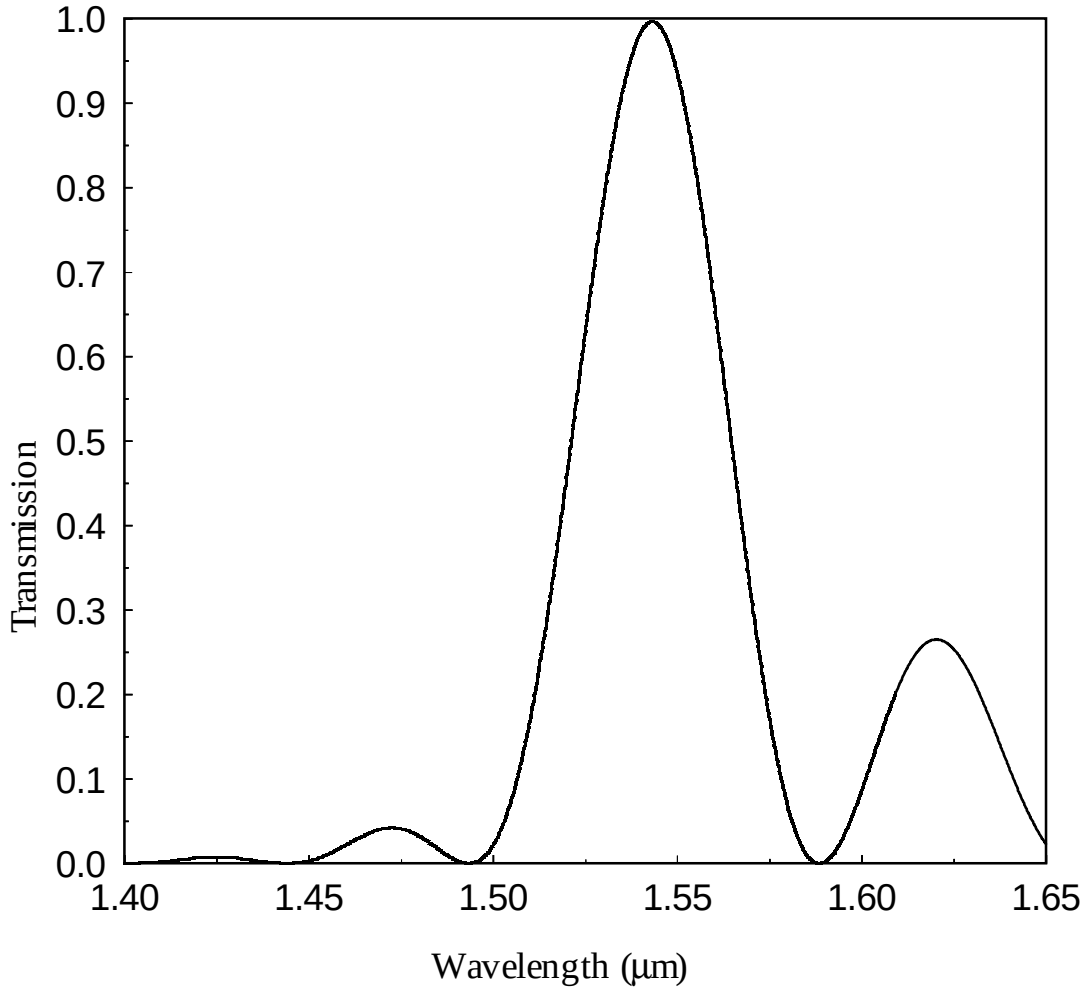

Figure 6.8 Transmission characteristic of 1.55 μm filter with fiber separation d = 15 μm. The parameters and materials of fibers are as defined in Table 6.2.

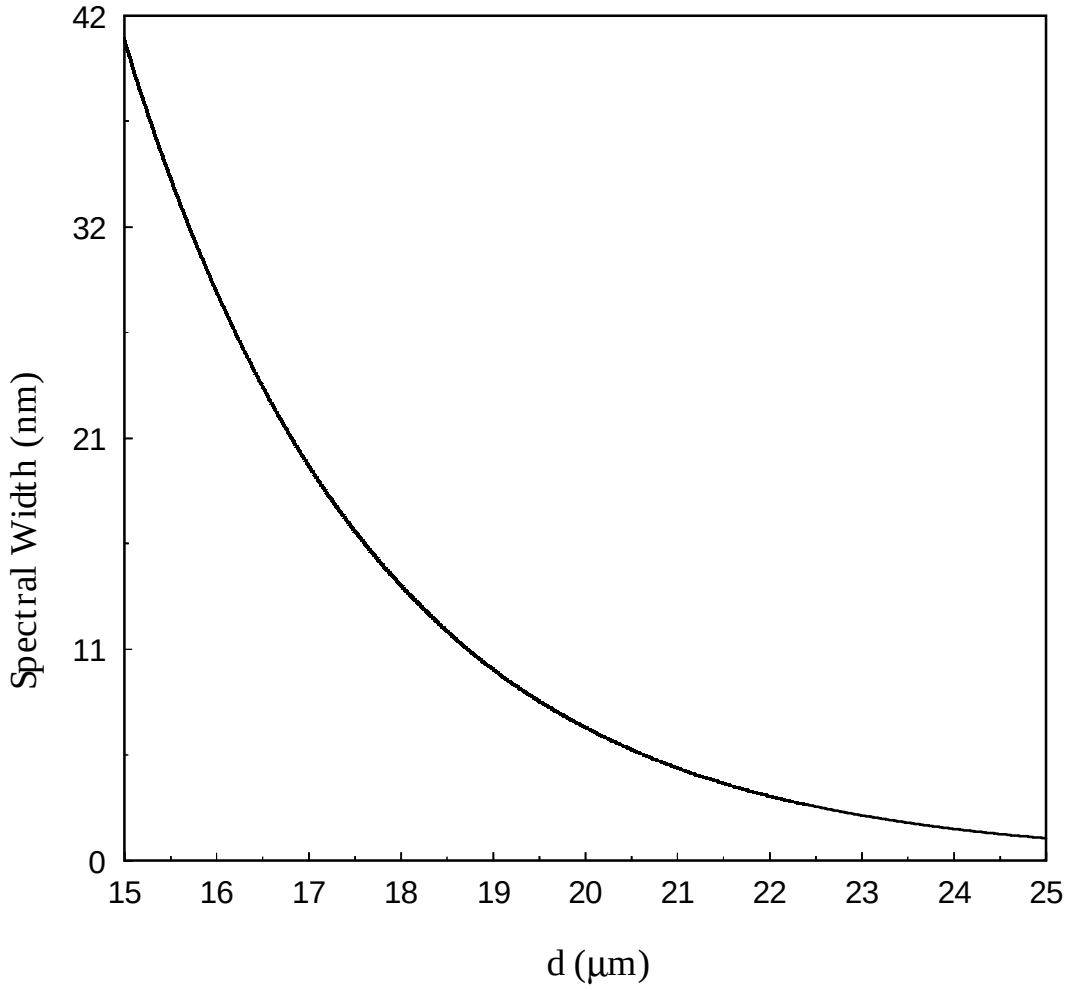

Figure 6.9 Variations of 3-dB spectral width versus fiber separation for 1.55 μm. The parameters and materials of fibers are as defined in Table 6.2.

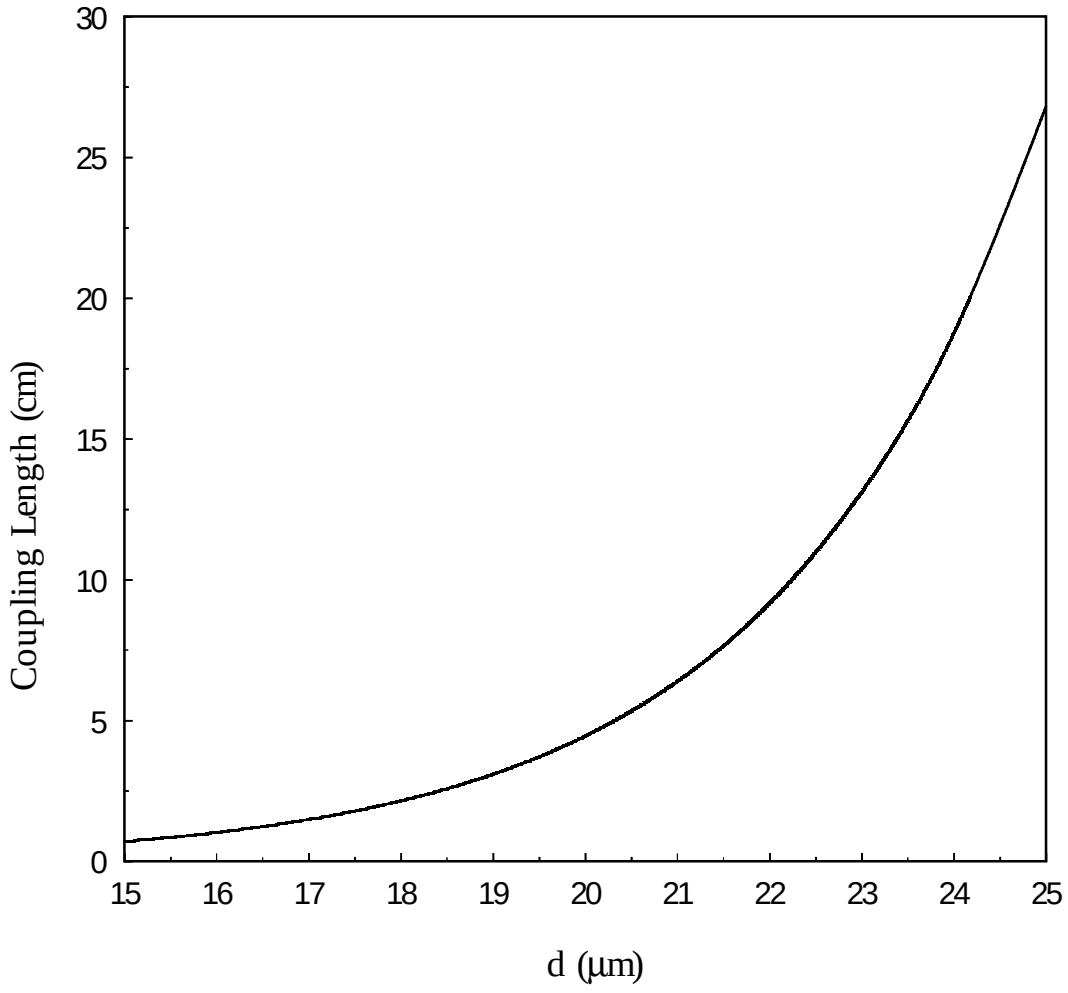

Figure 6.10 Variations of coupling length versus fiber separation for 1.55 μm. The parameters and materials of fibers are as defined in Table 6.2.

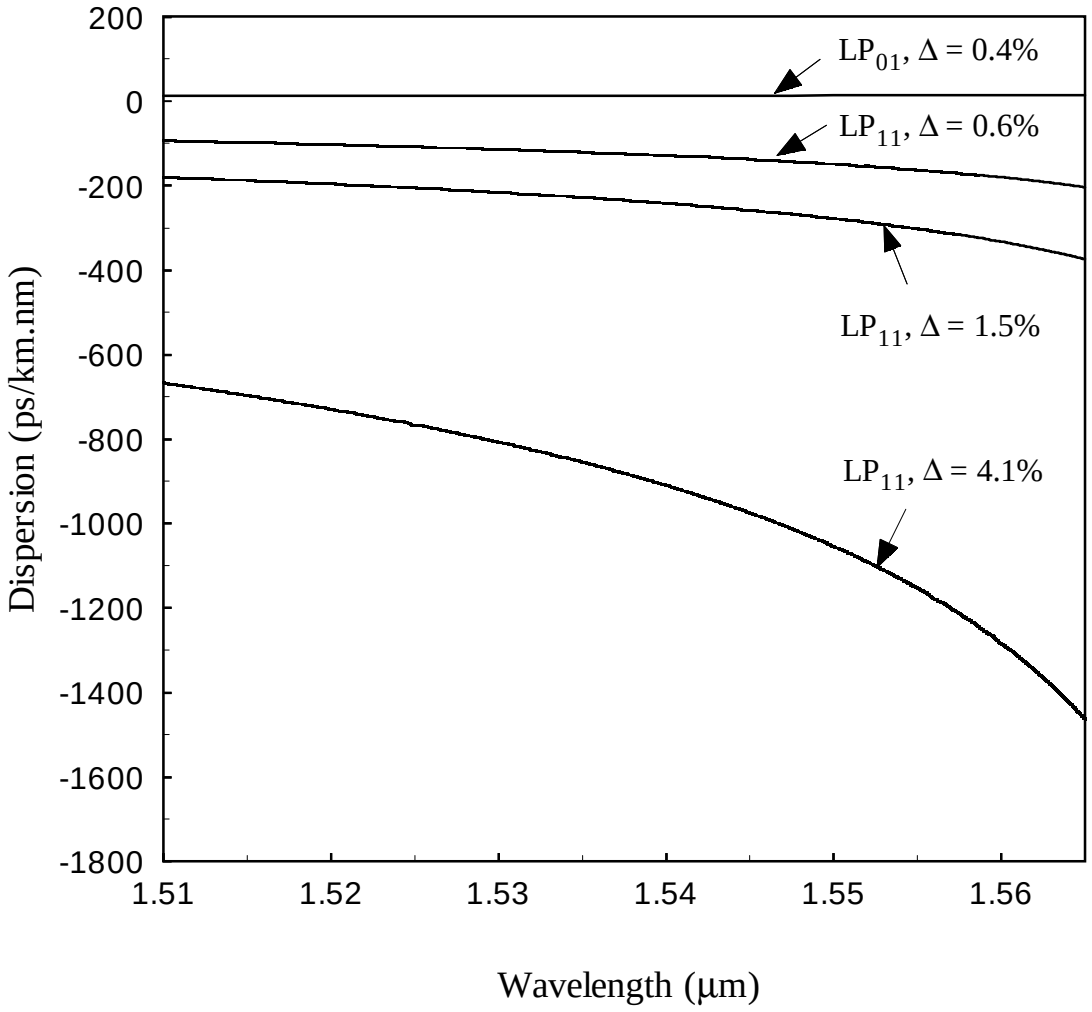

Figure 6.11 Variations of dispersion for LP_{01} mode of output fiber and LP_{11} mode of three dispersion compensating fibers with parameters and materials as defined in Table 6.3.

Table 6.3 Fiber parameters and material compositions for dispersion compensating (DC) fibers.

Fiber	Core Radius (μm)	Δ at λ = 1.55 μm	Core Material	Cladding Material
DC1	1.4	4.1%	16.9 m/o Na_20 32.5 m/o B_2O_3 50.6 m/o SiO_2	Pure Silica: annealed
DC2	2.4	1.5%	13.5 m/o GeO_2 86.5 m/o SiO_2	Pure Silica: annealed
DC3	3.8	0.6%	5.8 m/o GeO_2 94.2 m/o SiO_2	Pure Silica: annealed

m/o = mole percent

that the dispersion of the LP_{11} mode is negative and very large for index differences (Δ) more than 1%. As an example, for Δ = 1.5%, D_{11} = -277 ps/km.nm at 1.55 μm and all the dispersion accumulated over the length L of input fiber can be compensated with $|D_{01}/D_{11}| \approx 0.047L$ of the DC2 fiber.

Chapter 7

Conclusion

7.1 Conclusions

A two-fiber coupler operating based on LP_{01} - LP_{11} mode coupling has been proposed and studied using coupled-mode theory. One of the fibers used in the coupler structure is single mode supporting only the fundamental LP_{01} mode, while the other is a dual-mode fiber whose LP_{11} mode is phase matched with the LP_{01} mode of the first fiber at a desired wavelength. With appropriate choice of parameters, the coupler can be designed to function either as a narrowband spectral filter or a wideband mode converter. Using the coupled-mode theory of parallel dielectric waveguides, spectral characteristics of the proposed coupler were investigated. The effects of the pseudomode nature of LP_{11} mode on analytical solutions were examined. Design data and transmission characteristics for couplers with maximum coupling at λ = 1.33 μm and λ = 1.55 μm, two widely used wavelengths in fiber-optic communication, were calculated. The 3-dB spectral width of the 1.33 μm coupler varies between 1.5 nm and 13 nm when the fiber separation varies from 20 μm to 15 μm. The spectral width decreases almost exponentially with the fiber separation. Thus, a very narrowband filter as well as a wideband filter can be obtained by varying

the fiber separation. The coupling length is also strongly influenced by the fiber separation, increasing nearly exponentially. The side-lobe level of the 1.33 μm filter is about -10 dB for d = 20 μm, and is affected by the fiber separation but to a lesser degree. Filters designed for operation in the 1.3 μm window can find applications in wavelength division multiplexing.

Transmission characteristics of a filter designed for operation at 1.55 μm were also presented. Generally, at this wavelength, spectral width and side-lobe level are larger, and coupling length is smaller. The 1.55 μm coupler can find applications as both demultiplexer and mode converter. For mode conversion application, a wideband design is preferred. The coupler converts the LP_{01} mode of a 1.33 μm single-mode fiber into the LP_{11} mode of a dual-mode fiber with large negative dispersion at 1.55 μm. Design data for several dispersion compensating dual-mode fibers were also presented.

7.2 Suggestion for Further Work

Both fibers in the proposed coupler are matched-clad step-index fibers. The analysis presented here may be extended to study the LP_{01} - LP_{11} mode coupling when one or both fibers are multi-clad fibers such as W-fibers. This may result in even smaller spectral width. Another suggestion is to study mode coupling between LP_{01} and other higher-order modes such as LP_{02} modes. The higher order modes provide higher negative dispersion than LP_{11} mode.

Fabrication and measurement of the proposed coupler is a necessary step to be pursued. Although the simulation results are very optimistic, but the implementation of the proposed coupler will certainly require refinements and improvements which might be identified through experimental evaluations.

Appendix

A. Field Normalizations

The electric fields present in the two optical fibers are e_{1x} for the LP_{11} mode and e_{2x} for the LP_{01} mode, respectively. N_1 and N_2 are determined such that the power flows are normalized to unity.

Normalization N_1 :

$$N_1 = \frac{1}{2} n_1 Y_0 \int_{S_1} \left| e_{1x} \right|^2 dS_1 \tag{A.1}$$

$$= \frac{n_1 Y_0}{2} \int_0^{2\pi} \cos^2 \varphi_1 \, d\varphi_1 \left[\int_0^{a_1} \frac{J_1^2 (u_1 r_1)}{J_1^2 (U_1)} r_1 \, dr_1 + \int_{a_1}^{\infty} \frac{K_1^2 (w_1 r_1)}{K_1^2 (W_1)} r_1 \, dr_1 \right] \tag{A.2}$$

Using the characteristic equation for the LP_{11} mode given in (5.4) and with help of identities

$$K_1(z) = \frac{z}{2} \left(K_2(z) - K_0(z) \right) \tag{A.3}$$

and

$$J_1(z) = \frac{z}{2} \left(J_2(z) + J_0(z) \right) \tag{A.4}$$

N_1 is obtained as

$$N_1 = \frac{n_1 Y_0}{2} \frac{\pi a_1^2}{2} \frac{K_0(W_1)}{K_1^2(W_1)} \frac{V_1^2}{U_1^2} K_2(W_1) \tag{A.5}$$

Normalization N_2 :

$$N_2 = \frac{1}{2} n_2 Y_0 \int_{S_2} \left| e_{2x} \right|^2 dS_2 \tag{A.6}$$

$$= \frac{n_2 Y_0}{2} \int_0^{2\pi} d\varphi_2 \left[\int_0^{a_2} \frac{J_0^2(u_2 r_2)}{J_0^2(U_2)} r_2 \, dr_2 + \int_{a_2}^{\infty} \frac{K_0^2(w_2 r_2)}{K_0^2(W_2)} r_2 \, dr_2 \right] \tag{A.7}$$

Using the characteristic equation for the LP_{01} mode given in (5.5) and identities (A.3) and (A.4), N_2 is obtained as

$$N_2 = \frac{n_2 Y_0}{2} \frac{\pi a_2^2}{2} \frac{K_1(W_2)}{K_0^2(W_2)} \frac{V_2^2}{U_2^2} \tag{A.8}$$

The constant coefficients C_1 and C_2 in (4.1) and (4.2) are now given as

$$C_1 = 1/\sqrt{N_1} \tag{A.9}$$

$$C_2 = 1/\sqrt{N_2} \tag{A.10}$$

B. Coupling Coefficients

Coupling Coefficient κ_{12} :

From (3.8), we have

$$\kappa_{12} = \frac{\omega\varepsilon_0}{4}\left(n_2^2 - n_0^2\right) \int_{S_{\text{core 2}}} e_{1x}\ e_{2x}\ dS_2 \qquad \text{(B.1)}$$

The integration is performed over the core of fiber 2. In the core of fiber 2, the field e_{1x} of fiber 1 varies almost exponentially, while e_{2x} of fiber 2 behaves according to $J_0\,(u_2\ r_2)$. In terms of cylindrical coordinates, the above integral is represented as follows

$$\frac{1}{\sqrt{N_1\ N_2}} \int_0^{a_2} \int_0^{2\pi} \frac{J_0\left(u_2\ r_2\right)}{J_0\left(U_2\right)} \frac{K_1\left(w_1\ r_1\right)}{K_1\left(W_1\right)} \cos\varphi_1\ r_2\ dr_2\ d\varphi_2 \qquad \text{(B.2)}$$

The coordinates (r_1, φ_1) in terms of which the field e_{1x} is expressed must be transformed to the coordinates (r_2, φ_2) to facilitate the calculation of the above double integral. In doing so, we use the relationship [33]

$$K_m\left(ar_1\right) \begin{cases} \cos m\varphi_1 \\ \sin m\varphi_1 \end{cases} = \pm \sum_{p=-\infty}^{+\infty} (-1)^p\ K_{m+p}\left(ad\right)\ I_p\left(ar_2\right) \begin{cases} \cos p\varphi_2 \\ \sin p\varphi_2 \end{cases} \qquad \text{(B.3)}$$

In our case, $m = 1$ and $a = (W_1/a_1)$. Thus,

$$K_1\left(w_1\ r_1\right)\cos\varphi_1 = \sum_{p=-\infty}^{+\infty} (-1)^p\ K_{p+1}\left(w_1\ d\right) I_p\left(w_1\ r_2\right)\cos p\varphi_2 \qquad \text{(B.4)}$$

Now, substituting (B.4) in (B.2), we get

$$\sum_{p=-\infty}^{+\infty}(-1)^p \frac{K_{p+1}(w_1 d)}{J_0(U_2)K_1(W_1)} \int_0^{a_2} I_p(w_1 r_2)\, J_0(u_2 r_2)\, r_2 \int_0^{2\pi} \cos p\varphi_2 \, d\varphi_2 \, dr_2 \qquad \text{(B.5)}$$

But,

$$\sum_{p=-\infty}^{+\infty} \int_0^{2\pi} \cos p\varphi_2 \, d\varphi_2 = \begin{cases} 0 & \text{when } p = \pm 1, \pm 2, \ldots, \pm\infty \\ 2\pi & \text{when } p = 0 \end{cases} \qquad \text{(B.6)}$$

We further make use of the relation

$$\int z\ J_0(az)\ I_0(bz)\, dz = \frac{z}{a^2+b^2}\left\{ b\ J_0(az)\ I_1(bz) + a\ J_1(az)\ I_0(bz) \right\} \qquad \text{(B.7)}$$

and evaluate the integral $\int_0^{a_2}$ in (B.5). The result is

$$\int_0^{a_2} J_0(u_2 r_2)\ I_0(w_1 r_2)\ r_2\, dr_2 =$$

$$\frac{a_2}{\frac{U_2^2}{a_2^2}+\frac{W_1^2}{a_1^2}} \times \left\{ \frac{W_1}{a_1} J_0(U_2) I_1(W_1 a_2/a_1) + \frac{U_2}{a_2} J_1(U_2) I_0(W_1 a_2/a_1) \right\} \qquad \text{(B.8)}$$

Finally, using the characteristic equation for the LP_{01} mode given in (5.5) and the normalizations N_1 and N_2 in (A.5) and (A.8), the coupling coefficient κ_{12} is summarized as

$$\kappa_{12} = \sqrt{\frac{2(n_2^2 - n_0^2)}{n_1\ n_2}} \frac{K_1(w_1 d)}{K_1(W_2)\sqrt{K_0(W_1)K_2(W_1)}} \frac{U_1\ U_2}{a_1\ V_1} \frac{1}{U_2^2 + \overline{W}_1^2} \cdot \left\{ \overline{W}_1 K_0(W_2) I_1(\overline{W}_1) + W_2 K_1(W_2) I_0(\overline{W}_1) \right\} \qquad \text{(B.9)}$$

Coupling Coefficient κ_{21} :

From (3.8), we have

$$\kappa_{21} = \frac{\omega \varepsilon_0}{4}\left(n_1^2 - n_0^2\right) \int_{S_{\text{core}1}} e_{1x}\ e_{2x}\ dS_1 \qquad \text{(B.10)}$$

The integral term can be expressed as,

$$\frac{1}{\sqrt{N_1\ N_2}} \int_0^{a_1} \int_0^{2\pi} J_1(u_1\, r_1)\ J_1(U_1)\ K_0(w_2\, r_2)\ K_0(W_2) \cos\varphi_1\ r_1\, dr_1\, d\varphi_1 \qquad \text{(B.11)}$$

As before, the coordinates (r_2, φ_2) must be transformed to coordinates (r_1, φ_1). Using (B.3) with $m = 0$,

$$K_0(w_2\, r_2) = \sum_{p=-\infty}^{+\infty} (-1)^p\ K_p(w_2\, d)\ I_p(w_2\, r_1) \cos p\varphi_1 \qquad \text{(B.12)}$$

When the above expression is substituted in (B.11) and integrated with respect to φ_1 from *0* to 2π, it has a non-zero value only when $p = \pm 1$. Now, the integral in (B.11) is calculated as follows

$$2 \int_0^{2\pi} \cos^2 \varphi_1\, d\varphi_1 \int_0^{a_1} I_1(w_2\, r_1) \frac{J_1(u_1\, r_1)}{J_1(U_1)} \frac{K_1(w_2\, d)}{K_0(W_2)}\ r_1\, dr_1 \qquad \text{(B.13)}$$

We further use the relation

$$\int z\ J_1(az)\ I_1(bz)\, dz = \frac{z}{a^2 + b^2} \left\{ a\ J_2(az)\ I_1(bz) + b\ J_1(az)\ I_2(bz) \right\} \qquad \text{(B.14)}$$

and evaluate the integral $\int_0^{a_1}$ in (B.13). The result is

$$\int_0^{a_1} J_1(u_1 r_1)\, I_1(w_2 r_1)\, r_1\, dr_1 =$$

$$\frac{a_1}{\frac{U_1^2}{a_1^2}+\frac{W_2^2}{a_2^2}}\left\{\frac{U_1}{a_1} J_2(U_1) I_1(w_2 a_2)+\frac{W_2}{a_2} J_1(U_1) I_2(w_2 a_2)\right\} \qquad \text{(B.15)}$$

Finally, using the characteristic equation for the LP_{11} mode given in (5.4), the normalizations N_1 and N_2 in (A.5) and (A.8), and the identities (A.4) and

$$I_2(\overline{W}_2) = I_0(\overline{W}_2) - \frac{2}{\overline{W}_2} I_1(\overline{W}_2), \qquad \text{(B.16)}$$

the coupling coefficient κ_{21} is summarized as

$$\kappa_{21} = \sqrt{\frac{2(n_1^2 - n_0^2)}{n_1\, n_2}} \frac{K_1(w_2 d)}{K_1(W_2)\sqrt{K_0(W_1) K_2(W_1)}} \frac{U_1\, U_2}{a_2\, V_2} \frac{1}{U_1^2 + \overline{W}_2^2} \cdot \qquad \text{(B.17)}$$
$$\left\{W_1 K_0(W_1) I_1(\overline{W}_2) + \overline{W}_2 K_1(W_1) I_0(\overline{W}_2)\right\}$$

References

[1] P. Kaiser and D. B. Keck, “Fiber Types and Their Status” in “Optical Fiber Telecommunications II”, S. E. Miller and I. P. Kaminow, Eds., Harcourt Brace Jovanovich, 1991, ch. 2.

[2] H. Ishio, J. Minowa, and K. Nosu, “Review and Status of Wavelength-Division-Multiplexing Technology and Its Application”, J. Lightwave Technol., Vol. LT-2, No. 4, pp. 448-463, August 1984.

[3] S. B. Korovin, V. L. Smirnov, and A. V. Shmal'ko, “Narrow-Band Interference Holographic Filter Based on a One-Mode Fiber-Optic Light Guide”, Sov. Phys. Tech. Phys., Vol. 33, No. 12, p. 1466, December 1988.

[4] N. Imoto, “An Analysis for Contradirectional-coupler Type Optical Grating Filters”, J. Lightwave Technol., Vol. 3, No. 4, pp. 895-900, August 1985.

[5] W. P. Huang and J. Hong, “A Coupled-Waveguide Grating Resonator Filter”, IEEE Photonics Tech. Lett., Vol. 4, No. 8, p. 884, August 1992.

[6] M. Levy, L. Eldada, R. Scarmozzino, R. M. Osgood, Jr., P. S. D. Lin, and F. Tong, “Fabrication of Narrow-Band Channel-Dropping Filter”, IEEE Photonics Tech., Vol. 4, No. 12, p. 1378, December 1992.

[7] L. L. Buhl, R. C. Alferness, U. Koren, B. I. Miller, M. G. Young, T. L. Koch, C. A. Burrus, and G. Raybon, "Grating Assisted Vertical Coupler/Filter for Extended Tuning Range", Elect. Lett., Vol. 29, No. 1, p. 811, January 1993.

[8] O. Sahlen, M. Oberg, and S. Nilsson, "Tapered, Resonant DBR Transmission Filters", IEEE Photonics Tech. Lett., Vol. 5, No. 3, p. 327, March 1993.

[9] J. B. Soole, A. Scherer, Y. Silberberg, H. P. LeBlanc, N. C. Andreadakis, C. Caneau and K. R. Poguntke, "Integrated Grating Demultiplexer and PIN Array for High-Density Wavelength Division Multiplexed Detection at 1.5μm", Elect. Lett., Vol. 29, No. 6, p. 558, March 1993.

[10] S. R. Mallinson, "Fibre-coupled Fabry-Perot Wavelength Demultiplexer", Elect. Lett., Vol. 21, No. 3, pp. 121-122, January 1986.

[11] C. C. Chang, "Coupled-Waveguide Fabry-Perot Resonator", M.S. Thesis, Virginia Polytechnic Institute and State University, Blacksburg, VA, December 1992.

[12] T. Numai, "1.5 μm two-section Fabry-Perot Wavelength Tunable Optical Filter", J. Lightwave Technol., Vol. 10, No. 11, pp. 1590-1596, November 1992.

[13] J. Subias, R. Alonso, F. Villuendas, and J. Pelayo, "Wavelength Selective Optical Fiber Couplers Based on Longitudinal Fabry-Perot Structures", J. Lightwave Technol., Vol. 12, No. 7, pp. 1129-1135, July 1994.

[14] E. M. Dowling and D. L. MacFarlane, “Lightwave Lattice Filters for Optically Multiplexed Communication Systems”, J. Lightwave Technol., Vol. 12, No. 3, pp. 471-486, March 1994.

[15] K. Hirabayashi, H. Tsuda, T. Kurokawa, “Tunable Liquid-Crystal Fabry-Perot Interferometer Filter for Wavelength-Division Multiplexing Communication Systems”, J. Lightwave Technol., Vol. 11, No. 12, pp. 2033-2043, December 1993.

[16] N. Takato, A. Sugita, K. Onose, H. Okazaki, M. Okuno, M. Kawachi and K. Oda, “128-Channel Polarization-Insensitive Frequency-Selection-Switch Using High-Silica Waveguides on Si”, IEEE Photonics Tech. Lett., Vol. 2, No. 6, p. 441, June 1990.

[17] N. Takato, T. Kominato, A. Sugita, L. Jinguji,H. Toba and M. Kawachi, “Silica-Based Integrated Optic Mach-Zehnder Multi/Demultiplexer Family with Channel Spacing of 0.01-250 nm”, IEEE J. on Sel. Areas in Comm., Vol. 8, No. 6, pp. 1120, August 1990.

[18] M. Kuznetsov, “Cascaded Coupler Mach-Zehnder Channel Dropping Filter for Wavelength Division Multiplexed Optical systems”, J. Lightwave Technol., Vol. 12, No. 2, pp. 226-230, February 1994.

[19] M. S. Yataka, D. N. Payne, and M. P. Varnham, “All-fiber Wavelength Filters Using Concatenated Fused-Taper Couplers”, Electron. Lett., Vol. 21, pp. 248-249, 1985.

[20] R. Zengerle and O. G. Leminger, “Wavelength-selective directional coupler made of non-identical single mode fiber”, J. Lightwave Technol., Vol. LT-4, No. 7, pp. 823-827, July 1986.

[21] K. Okamoto and J. Noda, “Fiber-Optic Spectral Filters Consisting of Concatenated Dual-Core Fibers”, Electron. Lett., Vol. 22, pp. 211-212, 1986.

[22] A. Safaai-Jazi and J. C. McKeeman, “All-Fiber Spectral Filters With Nonperiodic Bandpass Characteristics and High Extinction Ratios in the Wavelength Range 0.8 μm < λ < 1.6 μm”, J. Lightwave Technol., Vol. 9, No. 8, pp. 959-963, August 1991.

[23] C. J. Chung and A. Safaai-Jazi, “Narrow-Band Spectral Filter Made of W-Index and Step-Index Fibers”, J. Lightwave Technol., Vol. 10, n 1, pp. 42-45, January 1992.

[24] Y. H. Ja, “Analysis of Optical Fiber Ring Resonators Using a Collinear 3x3 Fiber Coupler”, IEEE J. Quantum Electron., Vol. 30, No. 11, November 94.

[25] P. V. Adamson, “Fiber-Optic Spectral Filter”, Sov. Tech. Phys. Lett., Vol. 16, No. 11, pp. 853, November 1990.

[26] B. Moslehi and J. W. Goodman, “Novel Amplified Fiber-Optic Recirculating Delay Line Processor”, J. Lightwave Technol., Vol. 10, No. 8, August 1992.

[27] Z. M. Mao and W. P. Huang, “An ARROW Optical Wavelength Filter: Design and Analysis”, J. Lightwave Technol., Vol. 11, No. 7, July 1993.

[28] K. W. Cheung, D. A. Smith, J. E. Baran, and J. J. Johnson, “1 Gb/s System Performance of an Integrated, Polarization-Independent, Acoustically-Tunable Optical Filter”, IEEE Photonics Tech. Lett., Vol. 2, No. 4, pp. 271, April 1990.

[29] F. Tian, Ch. Harizi, H. Hermann, V. Reimann, R. Ricken, U. Rust, W. Sohler, F. Nehrmann, and S. Westenhofer, “Polarization-Independent Integrated Optical Acoustically Tunable Double-Stage Wavelength Filter in $LiNbO_3$”, J. Lightwave Technol., Vol. 12, No. 7, July 1994.

[30] D. A. Smith, M. M. Choy, A. d’Alessandro, J. E. Baran, and A. W. Rajhel, “Cascaded Acoustooptic/Fiber Fabry-Perot Filter With Finesse Over 2000”, IEEE Photonics Tech. Lett., Vol.5, No. 2, pp. 189, February 1993.

[31] J. R. Pierce, “Coupling of Modes of Propagation”, J. of Applied Physics, Vol. 25, No. 2, pp. 179-183, February 1954.

[32] H. Kogelnik, “Theory of Dielectric Waveguides” in “Integrated Optics”, T. Tamir, Ed., New York: Springer Verlag, 1975, ch. 2.

[33] A. W. Snyder and J. D. Love, “Optical Waveguide Theory”, Chapman and Hall, 1983.

[34] D. Gloge, “Weakly Guiding Fibers”, Appl. Opt., Vol. 10, p. 2252, 1971.

[35] A. Joseph Antos, and D. K. Smith, “Design and Characterization of Dispersion Compensating Fiber Based on LP_{01} Mode”, J. Lightwave Technol., Vol. 12, No. 10, pp. 1739-1744, October 1994.

[36] M. J. Adams, “An Introduction to Optical Waveguides”, New York: Wiley, 1981.

[37] G. Keiser, “Optical Fiber Communications”, McGraw-Hill Inc., 1991.

[38] A. Safaai-Jazi and L. J. Lu, “Accuracy of Approximate Methods for the Evaluation of Chromatic Dispersion in Dispersion-Flattened Fibers”, J. Lightwave Technol., Vol. 8, No. 8, pp. 1145-1150, August 1990.

Vita

Jagannathan Jyothikumar obtained his undergraduate degree in 1990 from the University of Madras, India, specializing in Electronics and Communications Engineering. Later, he continued his graduate studies and received his M.B.A from Virginia Polytechnic Institute and State University (VPI & SU). He also received his M.S. degree in Electrical Engineering from VPI & SU in June 1996. His current interests include Electromagnetics, Optics, Arts and Linguistics.